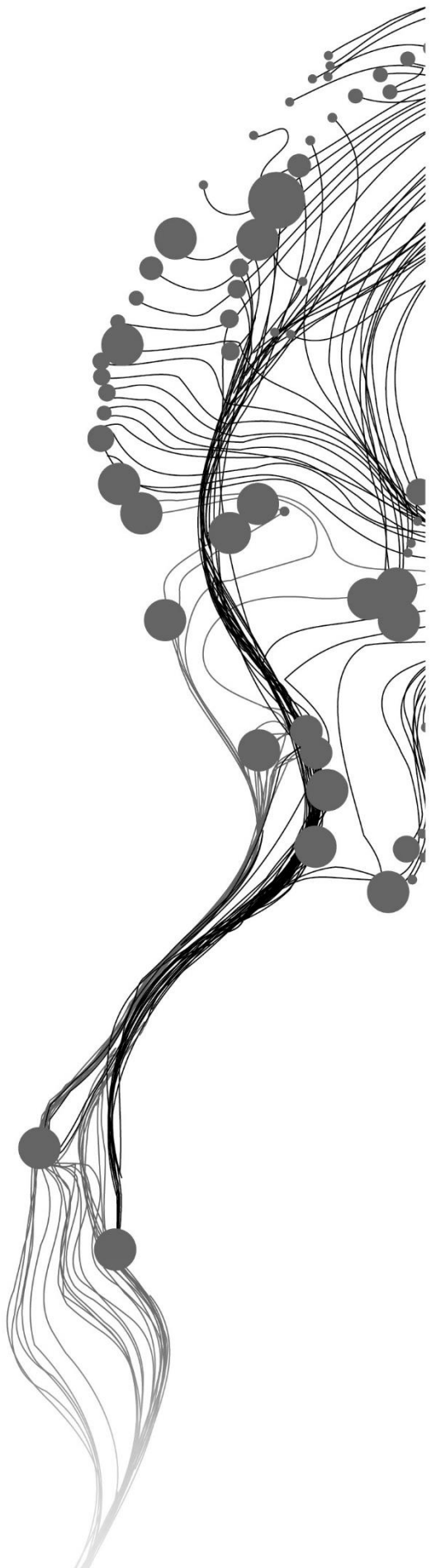


Comparing tree parameters extracted from UAV images and TLS data sets

JANA ERDBRÜGGER
June, 2017

SUPERVISORS:
ir. L.M. van Leeuwen - de Leeuw (Louise)
dr. Y.A. Hussin (Yousif)



Comparing tree parameters extracted from UAV images and TLS data sets

JANA ERDBRÜGGER

Enschede, The Netherlands, June, 2017

Thesis submitted to the Faculty of Geo-Information Science and Earth Observation of the University of Twente in partial fulfilment of the requirements for the degree of Master of Science in Geo-information Science and Earth Observation.

Specialization: Geo-information Science and Earth Observation for Environmental Modelling and Management (GEM)

SUPERVISORS:

ir. L.M. van Leeuwen - de Leeuw (Louise)

dr. Y.A. Hussin (Yousif)

THESIS ASSESSMENT BOARD:

prof.dr. A.K. Skidmore (Andrew)

Dr. Tuomo Kauranne (External Examiner, Lappeenranta University of Technology - Finland)

DISCLAIMER

This document describes work undertaken as part of a programme of study at the Faculty of Geo-Information Science and Earth Observation of the University of Twente. All views and opinions expressed therein remain the sole responsibility of the author, and do not necessarily represent those of the Faculty.

ABSTRACT

Forests are and have been an important source for raw materials and other services for humans. They are an important economical factor in many parts of the world and forestry has a long tradition managing this resource. Remote sensing is an important tool for the estimation and measurement of large forest areas and several methods have been developed over time.

Unmanned Aerial Vehicles (UAVs), also called drones, have become popular over the last years as an alternative and addition to other remote sensing approaches. In combination with commercial RGB cameras as sensors and photogrammetric processing of the UAV images have become more popular to complement data. With the strongly automatized image calibration, processing and point cloud generation from the Structure from Motion (SfM) process in combination with an Object based image analysis (OBIA) approach, individual trees and their parameter can be extracted.

The light detection and ranging (LiDAR) technology, particularly the terrestrial laser scanner (TLS), is used frequently in forestry for high precision in to generate accurate biomass estimations on tree level.

To determine if UAV derived tree parameter were as accurate as TLS derived measurements both data sets were compared to reference measurements. Manual measurements for the detection rate of trees and the DBH, airborne laser scanner (ALS) data for height reference. The influence of stand density and stand composition on the parameter extraction of both data sets was also analysed and compared.

The tree detection rate from the TLS data was very high (95 %). The number of trees delineated from the UAV data was slightly lower (87.4 %) and decreased further to just over half (56.3 %) of the number of trees counted in the field. There was a significant difference between height values from the reference ALS data and the height values extracted from UAV and TLS data sets. Height values from both data sets, UAV and TLS, were higher than the reference height values from the ALS data set.

TLS and UAV DBH values were not significantly different from the field measurements. The accuracy of UAV DBH estimations was higher (RMSE 0.124 m) than the accuracy obtained by the TLS (RMSE 0.334 m) but lower than the TLS DBH accuracy when excluding extreme outliers (0.079 m).

The UAV accuracy of both tree detection and DBH extraction accuracy were both significantly (negatively) influenced by higher density in stands and in stands with higher deciduous tree content. TLS tree detection and DBH value extraction was not influenced by stand composition but partly by stand density. Height values from both data sets were significantly influenced by stand density and composition

ACKNOWLEDGEMENTS

I thank my professors, family and friends for their support during my studies and am thankful for the opportunities I have been given.

TABLE OF CONTENTS

1.	Introduction and Research question.....	1
1.1.	Introduction	1
1.2.	Research problem	5
1.3.	Research objectives	5
1.4.	Research questions and hypotheses	6
2.	Methodology.....	9
2.1.	Data acquisition	9
2.2.	Data processing.....	14
2.3.	Data analysis	20
3.	Results.....	26
3.1.	Field measurements.....	26
3.2.	UAV image processing	27
3.3.	TLS data processing.....	28
3.4.	UAV and TLS data processing and tree detection	31
3.5.	Tree height extraction and accuracy.....	32
3.6.	DBH extraction and accuracy	35
3.7.	Forest type and stand structure influence	37
4.	Discussion.....	38
4.1.	Data acquisition and processing	38
4.2.	Tree detection and matching.....	46
4.3.	Tree height extraction and comparison.....	47
4.4.	DBH exrtaction and comparison	49
4.5.	Influence of stand composition and density	50
5.	Conclusions.....	52

LIST OF FIGURES

Figure 1: Dense point cloud constructed from UAV images through SfM process (with Pix4D).....	3
Figure 2: A dense TLS point cloud and the scanning positions (black dots) of a sparse Scots pine dominated forest stand coloured to show height (ground level (blue) to tree tops about 27 m above the ground level (red))......	4
Figure 3. Research Area by Amtsvenn, Ahaus, Germany showing the UAV flight areas (white line, white numbers) and sampling plots for TLS and field measurements (yellow diamonds).	10
Figure 4: left: TLS plot scanning positions. The circular plot (dotted grey line) was scanned from five positions (blue cylinders). One central scanning position and four evenly distributed outer scanning positions. Right: TLS RIEGL VZ-400 with additional mounted camera (image from RIEGL Laser Measurement Systems GmbH 2017)	10
Figure 5: UAV DJI Phantom 4 (image from DJI 2016)	12
Figure 6: Recorded flight plan for flight area 4. Red dots indicate the position of the UAV where an image was taken (measured by on-board GPS). The big red dot in the lower right corner indicates first picture taken from the UAV. The blue crosses mark the position of ground control points.....	12
Figure 7: Data processing steps, UAV data processing (red), TLS processing (blue), reference data (black); CPA-crown projection area, SfM- Structure from Motion, CHM-canopy height model, DBH – diameter at breast height	14
Figure 8: Upper figure: plot point cloud as obtained by combination of all five TLS plot scans (cropped just to include immediate plot surroundings). Middle figure: plot point cloud as above with marked individual tree as manually identified. Lower figure: isolated individual tree point cloud.	19
Figure 9: Data analysis steps for research question 1- 3 (Q 1-3). Red lines indicate UAV data input and output regarding only UAV and reference data comparisons, blue lines are assigned respective TLS regarding analysis steps, black lines show reference data input and UAV and TLS comparative output.	20
Figure 10: Analysis steps for Research question 4. Blue marks the TLS data input and relevant output, red marks the UAV data steps, black lines show reference data input.....	24
Figure 11: Distribution of field measured DBH (in meter) (including only the 14 sampling plots used in the analysis)	26
Figure 12: Results of the image calibration attempt of the 5 th UAV flight. Blue pyramids represent the recorded UAV GPS position when the picture was taken. Green pyramids show the calculated position after the Pix4D calibration (with additional manual tie points (green circles with pin) and GCPs (blue circles with pin)). Red pyramids signal images that could not be calibrated.....	27

Figure 13: Results of two DBH calculation methods (blue circles and red stars) without any filtering for the TLS data in relation to the field measured DBH (yellow 1:1 line). 28

Figure 14: Results of the both DBH calculation methods (blue circles and red stars) for the TLS data in relation to the field measured DBH (yellow 1:1 line) after excluding calculated TLS DBH values that had more than + 20 % deviations from the Field values. The blue and green line show the respective polynomial fit of DBH 1 and DBH 2. The Correlation coefficient of each set to the Field DBH is displayed in the upper left corner. 29

Figure 15: TLS DBH values calculated after the first method after running through filtering to eliminate noise. Stars (black) show the DBH results of trees that were not filtered while the circles (grey) indicate those values obtained after filtering out the outer 20 % of the stem point cloud. 30

Figure 16: The DBH values as calculated from the TLS tree data with the first calculation method. The crosses mark those DBH values that have been identified as outliers and were excluded from further analysis. 30

Figure 17: TLS (grey stars and line) and UAV (black crosses and line) height values for the matched trees compared to the ALS derived height values and the correlation values. 32

Figure 18: UAV height values (black stars and grey trend line) over the TLS height values for the matched trees and the correlation coefficient. 33

Figure 19: TLS DBH values (grey circles and dashed line) and UAV DBH values (black crosses and continuous line) for the matched trees over the field measurements of DBH. The correlation coefficient for the TLS values was calculated with (TLS) and without the five most prominent outliers ((TLS w/o outliers, outlier DBH values > 1 m). 35

Figure 20: left: Occlusion of structures/objects (see red circles) make recognition of connected structures (e.g. branches) difficult. Right: Intertwined tree stems that cannot effectively be separated and create errors especially when measuring DBH. 39

Figure 21: The occurrence of “shadows” of points behind objects (see red circles) add to general complexity of structures and make the recognition of interconnected and separated objects as well as the recognition of finer structures difficult. 39

Figure 22: UAV flight area 2 with irregularly spaced image acquisition points (red circles), GCPs (blue crosses) (background image source: Google Maps) 41

Figure 23: Image calibration results of flight area 1 and the DSM (upper left) and orthomosaic (upper right) derived from the dense point cloud generated in the SfM process (Data: University of Twente, 2017). Lower image: The image calibration results of the SfM process as obtained from the quality report by Pix4D: The grey rectangle marks the scope of the two upper maps Offset between initial (blue dots) and computed (green dots) image positions as well as the offset between the GCPs initial positions (blue crosses) and their

computed positions (green crosses) in the top-view (XY plane), front-view (XZ plane), and side-view (YZ plane). Red dots indicate disabled or uncalibrated images. Dark green ellipses indicate the absolute position uncertainty of the bundle block adjustment result.....42

Figure 24: Border area of the flight area 2 DSM (upper map) and orthomosaic (lower map). Showing trees that have not been properly reconstructed during in the SfM process and are therefore incorrectly or partly visible in the orthomosaic and DMS (red circles). The tree locations can be deduced from origin of the shadows of the tree stems in the orthomosaic. Stems of trees (blue circles) that normally should not be visible in the orthomosaic which should give a nadir view only of the tree crowns.....43

Figure 25: Crown delineation (red) in a low density coniferous plot.....44

Figure 26: Strongly intermingled crowns of a deciduous plot. Top: UAV derived orthomosaic with crown delineation (red), Bottom: TLS side view of trees of the same plot45

Figure 27: Small under-canopy trees (red) are occluded from above by the crowns of higher surrounding trees (black) and make a recognition in the UAV images impossible.....46

Figure 28: Flight plan (green line and red image taking positions) and GCPs (blue crosses) for UAV flight area 1 C

Figure 29: Flight plan (green line and red image taking positions) and GCPs (blue crosses) for flight area 3 C

Figure 30: Flight plan (green line and red image taking positions) and GCPs (blue crosses) for flight area 5D

LIST OF TABLES

Table 1: Classification criteria for the stand composition and stand density.....	25
Table 2: Descriptive statistics of data acquisition and processing for all sampling plots included in the analysis	26
Table 3: Calibration results for UAV image calibration process: number of images, number and percentage of calibrated images and the root mean squared error (RMSE) of the geo-referencing with the ground control points (GCPs). For flight area 5 (marked red) no RMSE error was calculated since no satisfactory image calibration was reached.	27
Table 4: Number of trees in remaining sampling plots, field measured (Field), TLS extracted (TLS and number of tree tops/crowns identified from the UAV data (UAV) in the plot area (crowns) and the number of trees that were successfully matched (matched) to the field and TLS positions as well as the mean distance of matched UAV tree positions to the TLS positions.....	31
Table 5: Plot-wise UAV, TLS and ALS height means and standards deviations of matched trees.....	34
Table 6: Plot-wise mean and standard deviation of height differences between TLS and ALS, UAV and ALS, UAV and TLS	34
Table 7: Plot-wise UAV, TLS and field measured DBH (and CPA for UAV) means and standards deviations of matched trees.....	36
Table 8: Plot-wise mean and standard deviation of DBH differences between TLS and field measurements, UAV and measurements, UAV and TLS	36
Table 9: Number of matched trees per composition and density	37
Table 10: Results of multiple linear regression analysis with dummy variables. Results displayed are adjusted R^2 (R^2 adj., light grey) and p-values for the variables. The variables were: for the stand composition, mixed (mix.) and deciduous (dec.) over the coniferous model; for the stand density, medium (med.) and high (high) over the low model. P-values higher than the chosen $\alpha=0.05$ are marked in dark grey ($p\text{-value} > \alpha$).....	37
Table 11: Standard Deviation (StDev) for scan registration in TLS plots. Calculated by using reflectors as tie points for scan registration by using a least square approach in RiSCAN PRO.	B
Table 12: Composition class, density class and number of matched trees per plot.....	E
Table 13: Results of regression analysis combining density and composition classes.....	G

1. INTRODUCTION AND RESEARCH QUESTION

1.1. Introduction

Forests are and have been an important source for raw materials and other services for humans. They are an important economical factor in many parts of the world and forestry has a long tradition managing this resource (West 2009). Apart from the raw materials like wood and fruits, forests also fulfil other highly important roles. They act as habitats for a large range of species. They are an integral part in the nutrient cycles and have a large impact on water cycles as well as sequester carbon dioxide from the atmosphere (Wirth et al. 2009).

In times of climate change the carbon sink function of forests has become an important function to reduce the emission of greenhouse gases (GHGs) and their impacts since the sequestered carbon is removed from the system. International treaties like the Kyoto Protocol take forests and their functions as one of the key factors in mitigating emissions of GHGs (Rosenqvist et al. 2003).

Assessing the forest resources and their contained biomass is therefore an important task for many stakeholders from sub-national to international levels. To quantify this resource in terms of biomass and carbon stock information in forest inventories on an ever more detailed level, down to the individual trees, is a challenge also for researchers.

Different methods are being used for the determination of biomass and carbon stocks. The most exact approach being destructive sampling for which the tree is cut down, measured and weighed. This approach gives detailed information about the biomass and the stored carbon (West 2009). Nevertheless, this approach does not only limit the biomass determination to only once in time because of its destructive nature but is also highly impractical for large stands (West 2009; Ravindranath & Ostwald 2008).

For biomass and carbon stock estimations without cutting and weighing, allometric equations are used. They are usually based on tree parameters like Diameter at Breast Height (DBH) and height and their strong correlation to the total biomass (Ravindranath & Ostwald 2008; West 2009; Laar & Akça 2007). While the DBH of a tree is still relatively easy to measure, the height is often more difficult to determine, especially within a forest (West 2009). Nevertheless, to determine tree volume and ultimately the biomass, the height is an important factor for accurate biomass estimations (Ravindranath & Ostwald 2008). The Crown Projection Area (CPA) is another measure that can also be used to estimate biomass and stands in relationship to DBH (Ravindranath & Ostwald 2008; Laar & Akça 2007). This relationship is particularly interesting for above canopy remote sensing approaches that use an object based image analysis (OBIA) to delineate single tree crowns in a forest canopy (Burnett et al. 2003).

Traditional forest measurement methods have been developed over centuries. While being well accepted and largely used these traditional, and often manual, measurement methods are not practical or relatively unprecise for the measurement of large forested areas. To measure and estimate the biomass of large forested areas the help of a wide range of remote sensing methods and technologies is being employed (West 2009; Rosenqvist et al. 2003).

Remote sensing is an important tool for the estimation and measurement of large forest areas and several methods have been developed over time (West 2009). Space based platforms carrying optical sensors and technologies like synthetic aperture radar (SAR) sensors and Light Detection and Ranging (LiDAR) systems are used for large scale forest estimations. They have been identified as being highly important tools also for the monitoring of forests for national and international carbon balances in order to comply with the Kyoto Protocol (Rosenqvist et al. 2003).

Remote sensing data can be used to extract important tree parameters which can be used with the appropriate models to estimate the forest biomass. These parameters, needed as model inputs, can, amongst other methods, be derived from aerial or satellite images. Using the CPA extracted from such an image the DBH can be estimated with reasonable results (Ravindranath & Ostwald 2008; Laar & Akça 2007). Even the height of trees can be extracted, for example through photogrammetric methods (Laar & Akça 2007; Dandois & Ellis 2010; West 2009).

When coming to very high resolution information down to individual tree levels satellite remote sensing technologies are reaching their spatial limit. The spatial resolution provided by satellite images is often not enough for the recognition of detail, for example when delineating tree crowns in a forest canopy. Cloud cover and shadows lead to occlusions and are a problem, especially in some geographical regions (Tang & Shao 2015). Other limitations are the revisiting time which restrains the possible time interval of image acquisition for a specific area and the maximum possible obtainable spatial resolution of approximately 0.5 m (Lucas et al. 2015).

1.1.1. UAV in forestry applications

To obtain very detailed information on tree level, especially in forests, the satellite based sensors are often not enough because of their spatial resolution or cloud cover. Unmanned Aerial Vehicles (UAVs), also called drones, have become rather popular over the last years as an alternative and addition to other remote sensing approaches (Dandois & Ellis 2013; Dandois & Ellis 2010; J. Zhang et al. 2016; Aasen et al. 2015; Gago et al. 2015; Stefanik et al. 2011). They do not have the above-mentioned limitations of traditional satellite remote sensing and have become reliable and economically affordable (Schiffman 2014). Advantages are the flexibility in time but also in choosing a spatial resolution by variation of flying height and the chosen sensor (W. Zhang et al. 2016). Especially in combination with simple commercial RGB cameras as sensors and a photogrammetric processing (using stereo vision) of the UAV images have become more popular to complement data where other remote sensing technologies are not available (Dandois & Ellis 2010).

The UAVs used for these ends are usually of the class of so-called micro drones. Though there is no universal nomenclature for drones yet established (Tang & Shao 2015) the micro-drones are loosely defined to be UAVs of up to 5kg including their payload. UAVs are usually distinguished into fixed wing or copter types. Fixed wing drones have usually a wider range while rotator drones are more manageable in restrained take-off and landing circumstances as well as being more flexible in terms of flight manoeuvres (Tang & Shao 2015). The extend of the area that can be covered by a UAV depends largely on the UAV type. Flight times and with its range can vary from 15 min to several hours depending on the drone type and the batteries.

UAVs can be used as a potential solution for the disadvantages of satellite images for forest measurements and monitoring. Images taken from a UAV platform have the advantage of delivering very high spatial resolution data, much higher than achievable from satellites (Dandois & Ellis 2010). Flying at low altitude this technology is a cloud-independent and images can be retrieved when needed and at the interval required

(Tang & Shao 2015). The technology for platforms and sensors has advanced a lot over recent years making this technology not only practical but also economically viable (Tang & Shao 2015; Dandois & Ellis 2010).

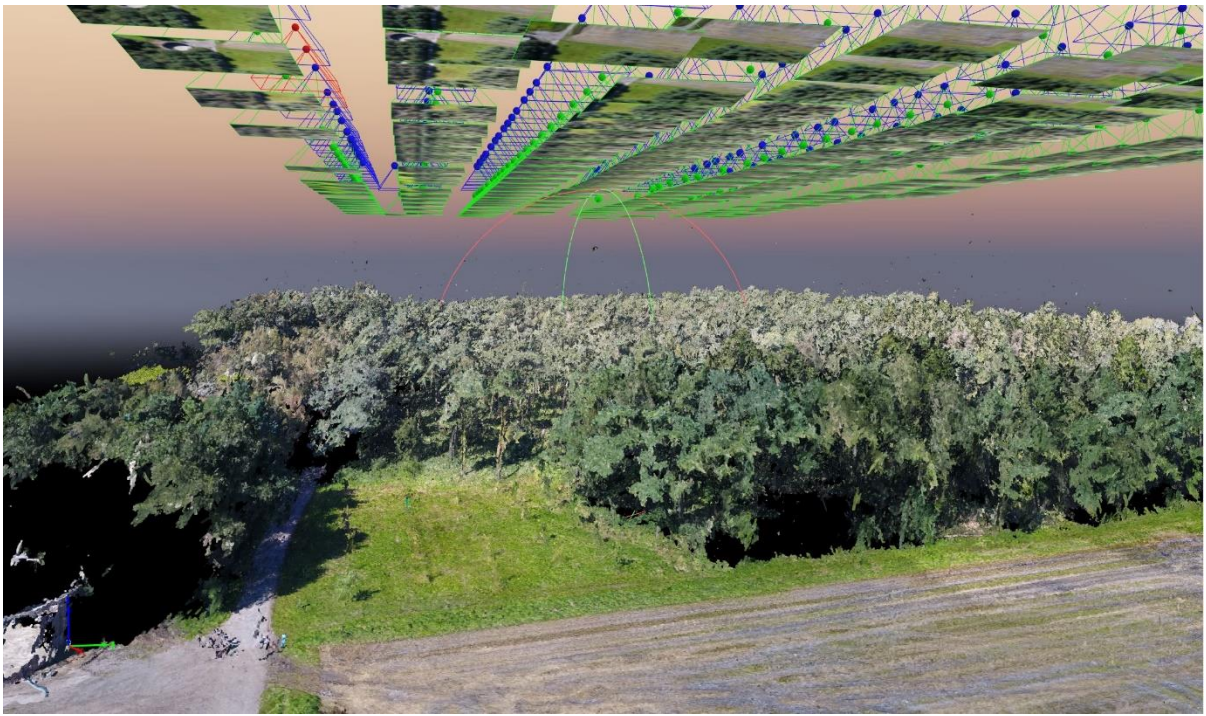


Figure 1: Dense point cloud constructed from UAV images through SfM process (with Pix4D)

Parallel to the development in drone technology there have been important developments made in the image processing domain of very high resolution imagery, improving and speeding up the automatic image processing, calibration and extraction of information with the Structure from Motion (SfM) method (Dandois et al. 2015; Dandois & Ellis 2010; Stefanik et al. 2011; Alcantarilla et al. 2012; Bay et al. 2006). Employing the SfM method the extraction of 3D information from overlapping (stereo pairs or multiple stereo) images is possible. Through the photogrammetric process a coloured point cloud can be extracted from the overlapping images (Figure 1) and orthomosaics as well as digital surface models (DSMs) can be constructed (Wallace et al. 2016; Dandois & Ellis 2010; Dandois & Ellis 2013).

These developments are very interesting also for forestry applications and research. The point cloud derived orthomosaics and DSMs can be used to delineate individual trees and extract CPA and height values that can be used in allometric equations to estimate biomass and carbon stocks.

Over the last years much research has been performed using drones for different applications in forestry and biology (Tang & Shao 2015; Schiffman 2014). Photogrammetrically processed high spatial resolution images taken from UAV platforms have for example been used to identify riparian buffer strip vegetation species (Husson et al. 2014). Zhang et al. (2016) have researched canopy variability and biodiversity, while forest biomass estimations and canopy phenology have been investigated by Dandois & Ellis (2013).

1.1.2. LiDAR for forestry applications

One of the most precise measurement methods used frequently in forestry is light detection and ranging (LiDAR) technology. The LiDAR sensor has been developed and improved further during the last years and is widely used as well in forestry (van Leeuwen & Nieuwenhuis 2010). From the generated point cloud (Figure 2) a variety of forest and tree parameters can be extracted (van Leeuwen & Nieuwenhuis 2010). Point clouds are created using laser pulses that hit objects on the ground or the ground itself where the measure of return time between the emitted pulse and its reflection is used to determine the distance to the reflecting object (van Leeuwen & Nieuwenhuis 2010).

Among the platforms used for LiDAR are the Airborne LiDAR or commonly called Airborne Laser Scanner (ALS) and Terrestrial LiDAR, also called Terrestrial Laser Scanner (TLS). The ALS is usually operated from a plane and it is traditionally used to generate Digital Surface and Terrain Models (DSM and DTM). The TLS can be used to extract detailed and precise information about trees (Liang et al. 2016; van Leeuwen & Nieuwenhuis 2010). The TLS is, as opposed to the ALS, stationary on the ground and used for plot-wise measurements. The high precision of this instrument allows to extract parameters from trees with high accuracy. The position of the TLS below the forest canopy allows for a very precise measurement of DBH but can also be used for volume as well as the general structure (van Leeuwen & Nieuwenhuis 2010; Kankare et al. 2016; Liang et al. 2016). Figure 2 shows an example of a TLS point cloud of forest. Height measurements are also possible although with some limitations because of occlusion by the canopy structure (Tansey et al. 2009). Because of its high precision in measurements (up to millimetre precision) this technology is often used for measurements to generate accurate biomass estimations on tree level and is also of high commercial interest in the forestry sector (Liang et al. 2016).

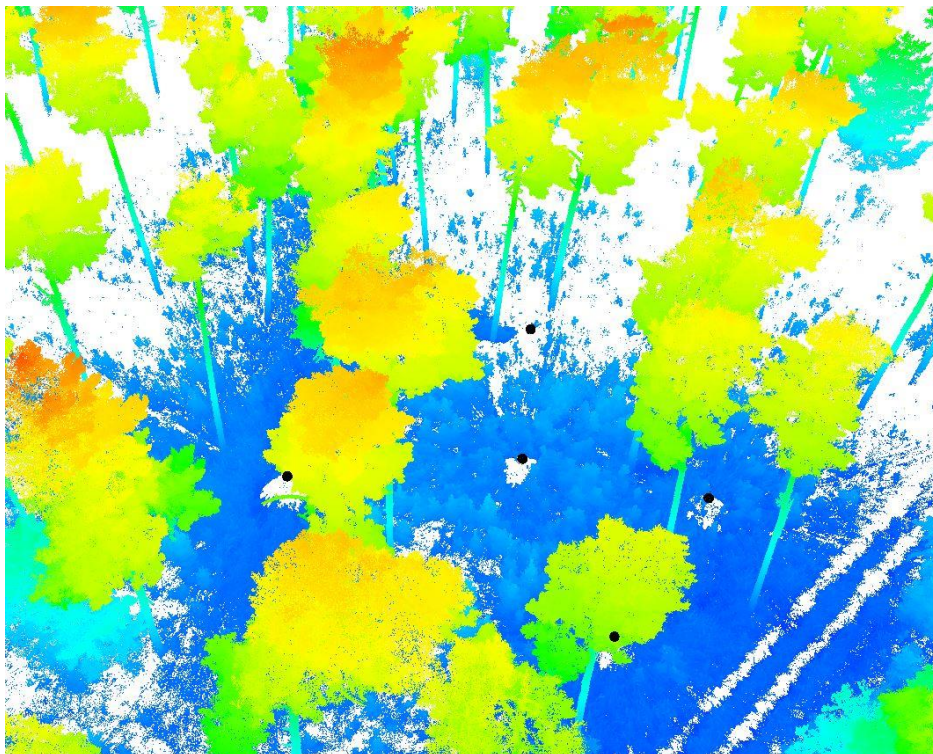


Figure 2: A dense TLS point cloud and the scanning positions (black dots) of a sparse Scots pine dominated forest stand coloured to show height (ground level (blue) to tree tops about 27 m above the ground level (red)).

1.2. Research problem

Though the TLS delivers high accuracy data of individual trees, one of the main disadvantages of this technology is that its operation is plot based. To assess larger areas, the measured parameters must be extrapolated from plots to a larger area. Extrapolation nevertheless, is a source for uncertainty since it is based on assumptions that may not be accurate.

UAVs on the other hand can cover and deliver data for larger areas. No extrapolation of the measured parameters is needed, which is one advantage of the use of UAVs and sensors for data acquisition.

The use of UAV images for remote sensing purposes has become quite popular in the forestry domain and is also economically highly attractive since commercial type UAVs with RGB cameras as sensors are much cheaper than other technologies (Dandois & Ellis 2010; Tang & Shao 2015; Schiffman 2014). Large areas can be covered in comparatively short time and at lower costs.

To decide on how useful information derived from commercial type UAV is, it is important to investigate how accurate the parameters extracted from UAV images are compared to technologies with as high accuracy like a TLS data.

The research in this study is focusing on the comparison of the tree parameters such as DBH or CPA and height extracted from UAV images and TLS data, which are commonly used for above ground biomass (AGB) estimations.

1.3. Research objectives

The general aim is to compare tree parameters extracted from UAV images by 3D photogrammetric methods and the same parameters extracted from TLS data sets.

Specific objectives are:

- Compare the ability of extracting individual trees from UAV and TLS data sets
- Compare tree parameters such as DBH or CPA and height extracted from TLS and UAV data set to reference data and with each other
- Assess and compare the influence of forest composition and stand density on the ability and accuracy of parameters extracted from UAV and TLS data sets.

1.4. Research questions and hypotheses

1. Does processing of the UAV and TLS data lead to the expected raw data for the analysis?

- Can all trees observed in the field be distinguished in the processed TLS data?
 - H_0 : The point cloud of the TLS plot permits the extraction of all individual trees with reasonable accuracy
 - H_1 : The point cloud of the TLS plot does not permit the extraction of all individual trees with reasonable accuracy
- Does the number of trees detected from the UAV data coincide with the number of trees observed in the field?
 - H_0 : The processed UAV data detect the same number of trees as observed in the field
 - H_1 : The processed UAV data does not detect the same number of trees as observed in the field
- Do the positions of trees from the TLS and the UAV data sets coincide?
 - H_0 : There is a significant difference in the position of detected trees from TLS and UAV data.
 - H_1 : There is no significant difference in the position of detected trees from TLS and UAV data.

2. Is there a significant difference between the UAV derived height values, TLS derived height values and the ALS reference height values?

- Is there a significant difference between the UAV extracted height and the height from the canopy height model derived from ALS?
 - H_0 : There is a significant difference in the height of the trees from the UAV data and the height derived from ALS.
 - H_1 : There is no significant difference in the height of the trees from the UAV data and the height derived from ALS.
- Is there a significant difference between the TLS derived height values and the height from the canopy height model derived from ALS?
 - H_0 : There is no significant difference in the height of the trees from the TLS data and the height derived from ALS.
 - H_1 : There is a significant difference in the height of the trees from the TLS data and the height derived from ALS.

- Is there a significant difference between the TLS derived height values and the height values derived from the UAV data?
 - H_0 : There is no significant difference in the height of the trees from the TLS data and the height from the UAV data.
 - H_1 : There is a significant difference in the height of the trees from the TLS data and the height from the UAV data.

3. Is there a significant difference between the UAV derived DBH values, TLS derived DBH values and the DBH values from the field measurements?

- Is there a significant difference between the DBH estimated from the CPA measured from the UAV data set and the field measured DBH?
 - H_0 : There is a significant difference in the DBH between the field measurements and the DBH derived from the CPA from the UAV data.
 - H_1 : There is no significant difference in the DBH between the field measurements and the DBH derived from the CPA from the UAV data.
- Is there a significant difference between the DBH derived from the TLS data set and the field measured DBH?
 - H_0 : There is a significant difference in the DBH and form of detected trees from field measurements and TLS data.
 - H_1 : There is no significant difference in the DBH and form of detected trees from field measurements and TLS data.
- Is there a significant difference between the DBH estimated from the CPA measured from the UAV data set and the TLS derived DBH?
 - H_0 : There is a significant difference in the DBH and form of detected trees from TLS and UAV data.
 - H_1 : There is no significant difference in the DBH and form of detected trees from TLS and UAV data.

4. Do forest type and structure influence the tree and its parameters (i.e., height and DBH) extracted from UAV and TLS data?

- Does the **stand composition** influence the **tree detection** from the TLS and UAV data set?
 - H_0 : There is no significant difference in the tree detection from the TLS and UAV data from coniferous, mixed and broadleaf stands.
 - H_1 : There is a significant difference in the tree detection from the TLS and UAV data from coniferous, mixed and broadleaf stands.
- Does the forest **stand density** influence the **tree detection** from the TLS and UAV data set?
 - H_0 : There is no significant difference in the tree detection from the TLS and UAV data from sparse and dense stands.
 - H_1 : There is a significant difference in the tree detection from the TLS and UAV data from sparse and dense stands.
- Does the **stand composition** influence the tree **height** extraction from the TLS and UAV data set?
 - H_0 : There is no significant difference in the tree height detection from the TLS and UAV data from coniferous, mixed and broadleaf stands.
 - H_1 : There is a significant difference in the tree height detection from the TLS and UAV data from coniferous, mixed and broadleaf stands.
- Does the forest **stand density** influence the tree **height** extraction from the TLS and UAV data set?
 - H_0 : There is no significant difference in the tree height detection from the TLS and UAV data from sparse and dense stands.
 - H_1 : There is a significant difference in the tree height detection from the TLS and UAV data from sparse and dense stands.
- Does the **stand composition** influence the **DBH** extraction from the TLS and UAV data set?
 - H_0 : There is no significant difference in the DBH detection from the TLS and UAV data from coniferous, mixed and broadleaf stands.
 - H_1 : There is a significant difference in the DBH detection from the TLS and UAV data from coniferous, mixed and broadleaf stands.
- Does the forest **stand density** influence the **DBH** extraction from the TLS and UAV data set?
 - H_0 : There is no significant difference in the DBH detection from the TLS and UAV data from sparse and dense stands.
 - H_1 : There is a significant difference in the DBH detection from the TLS and UAV data from sparse and dense stands.

2. METHODOLOGY

The methodology is divided into three main parts.

Data acquisition is covering general information about the research area, the sampling design and the fieldwork procedures for UAV, TLS and manual measurements. It also includes information on the acquisition of additional LiDAR data for elevation information.

The processing of the data sets will be explained; TLS point cloud processing to obtain the parameters for individual trees; the work flow for the UAV data to obtain individual tree parameters; processing of the LiDAR reference data; Above Ground Biomass (AGB) estimations from parameters of the UAV and TLS data set.

The third part is concerned with the data analysis and comparison of the data sets in order of the posed research questions.

2.1. Data acquisition

The data acquisition description comprises of: the general description of the research area; the two main field work parts, TLS and manual measurements as well as UAV image acquisition; and the sourcing of additional DTM and reference DSM.

2.1.1. Research area

The study area (about 0.5 km²) consists of patches of forest with mixed tree species (Figure 3). It is located on the border of the Netherlands and Germany, by Amtsvenn, close to the city of Gronau, Nordrhein-Westfalen, Germany (: 32558395 m E, 5782262 m N, UTM 32 N, ETRS89).

The research area consists of several forest stands within an agricultural area (Figure 3). These stands are managed on an informal basis and show different densities, stand compositions and growing stages. The most common tree species were Beeches (*Fagus sylvatica*), Scots pines (*Pinus sylvestris*), Oaks (*Quercus robur*, *Quercus petraea*), Alders (genus *Alnus*) and Birches (genus *Betula*). The identification was done on a common name basis and not distinguishing sub-species.

A stratified random sampling method was employed to select plot sites within in the research area (Figure 3). The plot based sampling was chosen because of the TLSs plot based functioning. A relatively high number of potential plot sites were generated. In the field, some of these plots had to be skipped because of inaccessibility. Dense and thorny undergrowth of up to 2 m height inhibited the access with the TLS and would also have occluded large parts of the plot. This lead to some bias for some forest patches.

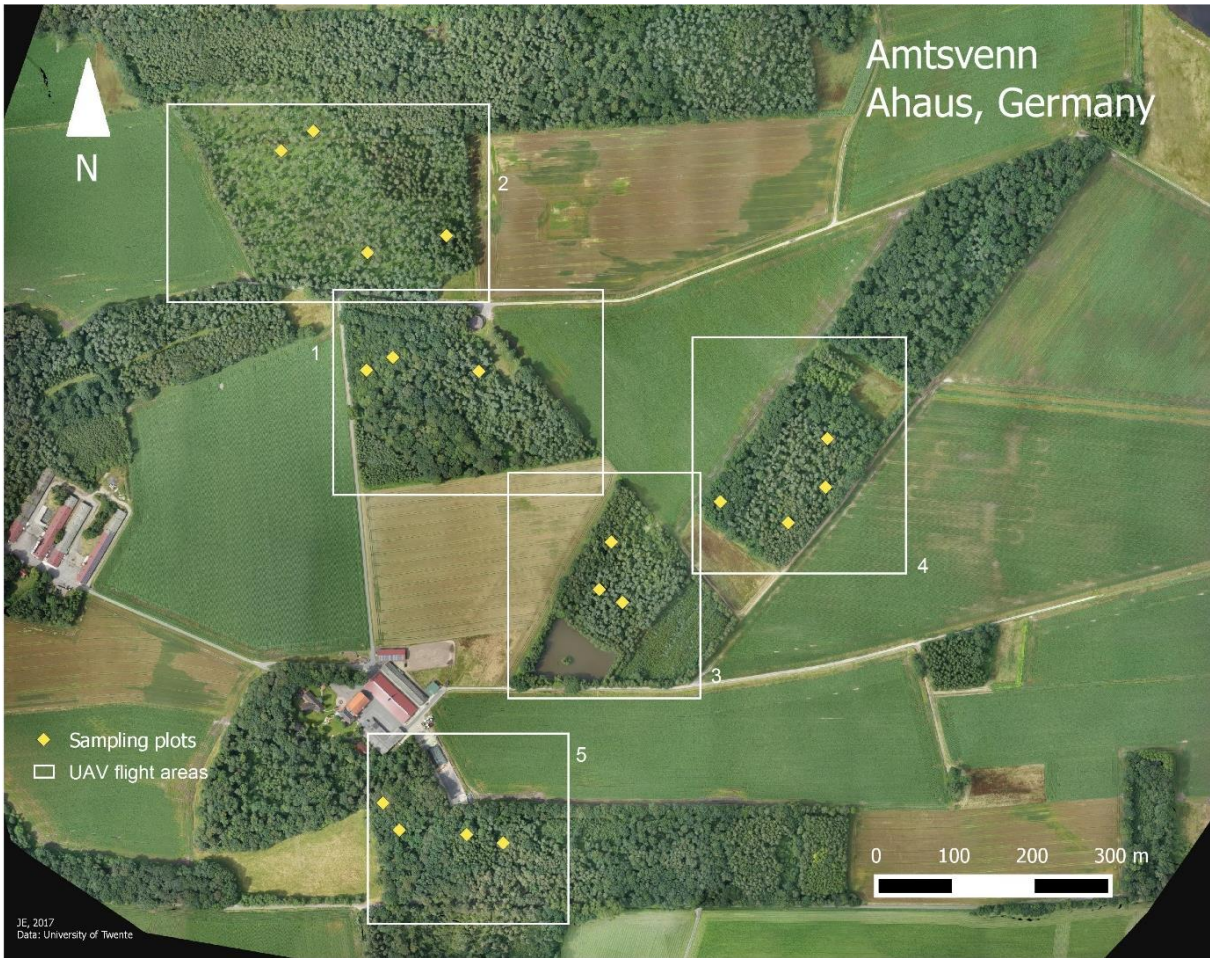


Figure 3. Research Area by Amtsvenn, Ahaus, Germany showing the UAV flight areas (white line, white numbers) and sampling plots for TLS and field measurements (yellow diamonds).

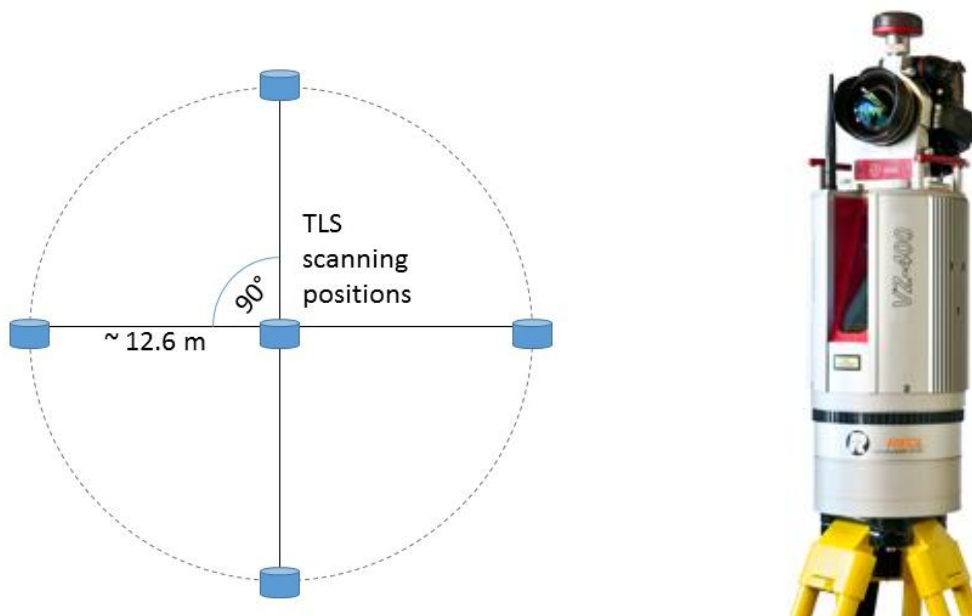


Figure 4: left: TLS plot scanning positions. The circular plot (dotted grey line) was scanned from five positions (blue cylinders). One central scanning position and four evenly distributed outer scanning positions. Right: TLS RIEGL VZ-400 with additional mounted camera (image from RIEGL Laser Measurement Systems GmbH 2017)

2.1.2. TLS and manual data acquisition

The sampling unit for the comparison are individual trees but for practical reasons sampling plots were established to do the field work with the TLS and for the manual field measurements. The plot based TLS scanning procedure allowed to scan several trees within the plot at the same time while the scanning of individual randomly selected trees in the research areas would have been unfeasible both time- and involved labour-wise.

The plots were circular of 500 m² (12.62 m radius) (Liang et al. 2016). Each plot was scanned by the TLS from 5 scanning positions with one central plus four outer scanning positions distributed at 90° from each other and at approximately 12.6 m from the centre spot (Figure 4). From practical experience this formation of scanning positions resulted in the most complete scans of forest plots (Calders et al. 2015).

The TLS used for the fieldwork was a Riegl VZ400 with an additional camera on top (Figure 4). The TLS was mounted on a tripod. The angular resolution used for scanning of the plots was of 0.0007° for a resolution of 7 cm at 100 m distance over a vertical angle of 130° (3D Laser Mapping Ltd. 2012). For the later merging of the five scans of a plot, cylindrical retro-reflectors were evenly distributed in the plot to be used as fix points in the registration. The cylindrical form of the retro-reflectors ensured that they were visible from all scanning positions if they were not occluded by other objects. The special reflective surface was recognized by the TLS and the position of the reflectors was marked in the saved data set.

The manual measurements were done at the TLS plots as well. All trees in the plot were measured with a Diameter tape at breast height (1.30 m from the base of the tree trunk, accurate to millimetre level). The measurements were recorded along with the species of the trees to be able to separate the plots into the categories of coniferous, deciduous or mixed forest types. Only trees with a diameter equal or above 10 cm were recorded. The 10-cm diameter threshold value was chosen since it is generally assumed that the forest biomass contribution of trees with smaller DBH is negligible in most cases (Brown 2002). The threshold also excludes many small trees that are below the canopy and cannot be seen from above on the UAV images.

2.1.3. UAV data acquisition

The UAV flights were done with a DJI Phantom 4 with an integrated RGB camera with a 12.4 MP resolution (Figure 5). The UAV data collection was done in five flights over the forest patches of the research area. All flight parameters were the same for all the flight plans. The flying height was at 70 m (above the starting point of the UAV). The front overlap between images was 80% and the side overlap was 60%. The camera was oriented in a Nadir direction. The flight plan was chosen relatively wide to make sure no edge effects would occur in the research area (Figure 6 and Annex 3). The flights were done in the late morning to mid-day during late summer.

Although the UAV had an integrated GPS, used in flight control, the information was not very accurate. For a high-accuracy geo-referencing of the UAV images four or more Ground Control Points (GCPs) were set for each flight area (Figure 6, blue crosses). The location for those GCPs was selected to have a relatively unobstructed view of it from the air and therefore be visible from more than one image. The GCPs were distributed close to the corners around the forest patches. The GCPs were placed on the ground and then georeferenced with a differential GPS. The accuracy of the coordinates of these GCPs was about 2.5 cm.



Figure 5: UAV DJI Phantom 4 (image from DJI 2016)



Figure 6: Recorded flight plan for flight area 4. Red dots indicate the position of the UAV where an image was taken (measured by on-board GPS). The big red dot in the lower right corner indicates first picture taken from the UAV. The blue crosses mark the position of ground control points.

2.1.4. Digital Terrain and Surface model

A Digital Terrain Model (DTM) was used for the ground elevation data. Although it is in theory possible to derive a DTM from the UAV data, the results of previous studies (Ota et al. 2015; Wallace et al. 2016) do indicate a relatively low accuracy in UAV image derived DTMs even in relatively open forests.

Additionally, a Digital Surface Model (DSM) was acquired as well to be used as reference for the TLS and UAV data. For this study the DTM and DSM were kindly provided by the Geobasisdaten der Kommunen und des Landes Nordrhein-Westfalen (NRW). The obtained DTM is from a filtered ALS data set and comes at a resolution of 1 to 4 points per square meter while the DSM consists of first pulse returns of at least 4 points per square meter (Bezirksregierung Köln 2016). The accuracy of the elevation data is about 20 cm but might be higher in forests (Bezirksregierung Köln 2016). The ALS data were obtained on the 29th of February in 2015 (GeoBasis NRW 2017).

2.2. Data processing

A general overview of data processing steps for the different data sets can be seen in Figure 7. The detailed explanation of individual processing steps is in the following sub chapters.

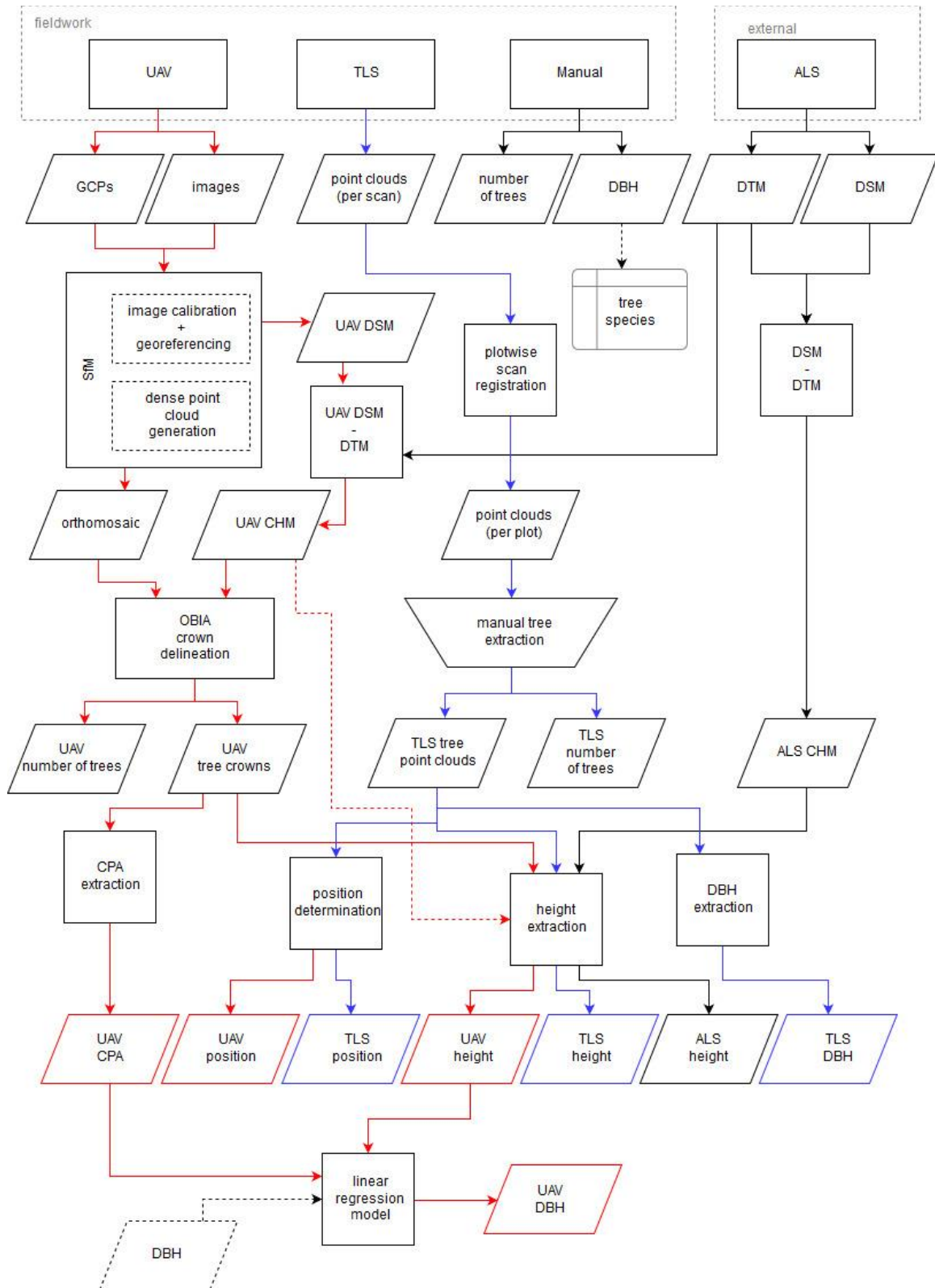


Figure 7: Data processing steps, UAV data processing (red), TLS processing (blue), reference data (black); CPA-crown projection area, SfM- Structure from Motion, CHM-canopy height model, DBH – diameter at breast height

2.2.1. Reference Canopy Height Model (CHM)

Manual height measurements in the forest are relatively difficult mainly because of occlusion of the tree tips from the ground (West 2009). To have a measure of the accuracy of UAV image derived heights a Canopy height model (CHM) was generated from the aerial LiDAR based DTM and DSM by subtracting DTM from DSM.

A limiting aspect of this CHM is that individual tree height estimates based on aerial LiDAR (resolution 3-4 points/m²) are usually underestimating the tree height by about 7-8% (Suárez et al. 2005). Nevertheless, they are considered more accurate than manual measurements (Suárez et al. 2005) and therefore present the best approximation for an accurate CHM.

2.2.2. UAV data processing

To obtain the tree parameters CHM and height from the UAV images the data were first processed using a Structure from Motion (SfM) method. The results from this step were then further processed using an Object based Image analysis approach (OBIA). Both procedures are explained in the following section.

2.2.2.1. Structure from Motion (SfM)

For the image processing of the images taken from the UAV the Structure from Motion (SfM) method was used to construct a point cloud as well as an orthomosaic.

The SfM method is a photogrammetric method which generates 3D point clouds from a large data set of overlapping images. To tie stereo images together tie points in each image are identified and described (Alcantarilla et al. 2012; Bolles & Baker 1987). Once these tie points are identified they are matched to the tie points in the other images of the scene (Bolles et al. 1987) and their fit is optimized by means of bundle adjustments (Dandois & Ellis 2010). Once the calibration of the images is done 3D points can be generated by triangulating their position from two or more images in which these points are visible (Bolles & Baker 1987).

The process of using Pix4D software is mostly automatic with some possibly necessary manual edits/corrections. Manual tie-points can be marked in the images both as addition to the automatically identified tie-points for improved image calibration and as GCPs. The georeferenced GCPs are included to refine the geo-referencing of the 3D point cloud.

The resolution of UAV images can be expressed in terms of the Ground Sampling Distance (GSD) which is the measure of how big one pixel of an image is on the ground. This determines the level of detail that can be represented in the image. Generally speaking, the larger the GSD the lower the pixel resolution (size) of an image is or the higher the distance to the object (or often, with UAV, to the ground) from which the image was taken (Dandois et al. 2015). Lower spatial resolution images have the advantage of needing less computing resources, especially for processing while images taken from higher positions include a larger ground area (Dandois et al. 2015). Higher resolution on the other hand allows for more details to be recognized in an image as well as in the 3D point cloud. However, the large amount of detail in images can make the tie-point identification difficult since it also adds to the general noise and complexity in an image. This is often the case with tree canopies because of their complex structure due to leaves, gaps in the canopy and irregularities in their growth form (Dandois & Ellis 2010).

For the SfM processing the UAV images from the research area were loaded into Pix4D and calibrated in a first step. After the first calibration, the GCPs were included and manually identified and marked in the images as well as the necessary tie points. A second calibration process was performed to optimize the general calibration of images as well as their spatial reference.

For the dense point cloud matching the point density was set to high and the number of minimum matches to generate a point was set to the minimum of just 2 images. Though this added some level of noise to the generated point cloud, this minimum of matches was necessary since otherwise many other points would not have been identified.

Before generating the orthomosaic and DSM in the last step, the point cloud was manually cleaned of obvious noise. Points that were clearly disconnected and “floating” far below and above the easily identifiable objects of the main point cloud were deleted from the data set. From the remaining point cloud an orthomosaic as well as a DSM were generated and exported.

The DSM data were normalized/converted to a Canopy height model by subtracting the aerial LiDAR DTM values from the obtained UAV DSM values (Annex 5).

2.2.2.2. Object based image analysis (OBIA)

The resulting orthomosaic and normalized Digital Surface Model (DSM) from the SfM process was then used in the identification of single trees using an Object-oriented Image Analysis (OBIA) approach. Since the orthomosaic and CHM from the UAV data were of very high resolution a limitation of the area was needed to reduce processing time. The central plot locations were identified and a radius of 25 m to account for the canopies of trees extending outside the sampling plot radius of 12.6 m and positional error from the GPS from the central plot locations was used to clip the area to be processed in the image analysis.

OBIA is a commonly used approach for image and elevation data segmentation and classification, particularly with very high resolution data (e.g. MacFaden et al. 2012; Richardson & Moskal 2011). It is based on meaningful objects as opposed to pixel classification. These objects consist of a group of pixels which often have similar values but can also be defined by other parameters such as the shape, size and texture of an object or its context (MacFaden et al. 2012). The defining properties of these objects are derived from expert knowledge (MacFaden et al. 2012). A tree crown can be such an object and can for example be defined by being at a certain height above ground, having a particular colour composition and a roughly circular shape (MacFaden et al. 2012). Many different approaches for using the knowledge to delineate tree crowns have been researched. A popular approach is to identify local maxima as tree tops and grow the tree crown objects around these maxima. Another approach is a valley-following delineation, basically a watershed-delineation based on an inverted Canopy height model (Jakubowski et al. 2013). The accuracy of the results depends highly on the research area and what kind of rule-set was created. Though the OBIA approach can be a highly efficient way of tree crown delineation, it is also sensitive to inaccuracies caused by insufficient or inaccurate knowledge used to develop a rule set.

The eCognition Developer software was used for the OBIA based tree crown delineation from the UAV data

The orthomosaic and CHM were resampled with a bilinear approach to a 10 cm by 10 cm spatial resolution to smooth over some of the small-scale noise that was not removed during the SfM process.

For the initial object creation, a multiresolution segmentation was performed based on the CHM and the orthomosaic. The multiresolution segmentation and creates objects of a defined scale based on automatically detected “natural” borders in the input data. For the first segmentation, a very small size was chosen obtaining an over-segmentation of the tree crowns. These small objects were then classified into “tree canopy” and “none-canopy” objects to separate out none-tree related objects (see e.g. MacFaden et al. 2012). The threshold chosen to filter out lower none-tree objects was based on observations in the field and set to 5 m for the mean elevation of an object.

A watershed approach as used by Jian Yang et al. (2014) was chosen to separate the crowns in the canopy. For this all objects in the canopy class were first merged and the watershed segmentation was then performed on the inverted DSM layer. To avoid too much over-segmentation an overflow criterion was included which resulted in the fusion of objects that consisted of less than a determined number of pixels. This overflow criterion was chosen by the estimation of the area of the smallest tree crowns in a plot.

The resulting objects were then evaluated and too large objects (under-segmented canopy) were broken up by another multiresolution segmentation. The parameters for this segmentation were chosen in a trial and error approach determining the best combination of parameters based on observations after several iterations testing several possible threshold values.

After achieving a satisfactory segmentation result the objects were filtered based in their roundness. Most of the filtered out none-round objects were slivers on the side of crowns while the rounder objects usually appeared on tree crown tops. To grow the tree tops to the approximate size of the whole crown the slivers were again segmented into very small objects and the tree tops were then grown in several loops into these small objects. To avoid the formation of unrealistic crown shapes and sizes, threshold conditions were set that limited the growing to maintain a relatively round shape and a size determined by the average crown size estimated visually for each plot.

For the last steps, a circular mask was used to remove “unnatural” edges and smooth the outer crown boundaries. Small gaps within the crowns were filled in to create more realistic tree crown shapes (MacFaden et al. 2012). The resulting crowns and their centre points were exported as shape files.

The tree crowns were imported in ArcGIS to calculate the individual Crown projection areas. The centre point of each delineated tree crown to be used as the tree position to be compared to the TLS tree positions. It was assumed that the stem position coincides with the centre position of the tree crown.

The allometric relationship between DBH, height and crown projection area (Widłowski et al. 2003; Rutishauser et al. 2013) was used to derive a general model for the DBH estimation from CPA and height values (Rasel et al. 2017). Two linear regression models, one using only CPA values and the other combining CPA values with height values, were fitted to the field measured values thus estimating the research areas specific allometric relationship. These linear regression models were based on 50 sample trees that were selected from all sample plots. The selection of sample trees was done by selecting 2 to 5 well delineated trees from each sample plot. The decision which trees were included was based on visual inspection of the delineations.

The fit of the models was evaluated by calculating the R^2 values and the model with better fit was selected for the DBH calculation.

2.2.3. TLS data processing

The primary processing of the TLS data set was done using the RiSCAN PRO software.

All five scans belonging to one plot were uploaded into a project. With the help of the retro-reflectors, which served as anchor points, the scans were registered and set into relation with each other. The correct registration of the scans was done by matching the retro-reflectors, also called tie points, in each scan to their respective counterparts in the other scans. The fit was done by calculating the standard deviation of the distance of the reflectors to each other.

The mean deviation for the registration of point clouds was 0.021 m with a range from 0.011 to 0.060 m (Annex 2). These values are slightly higher than those obtained by other researchers (see Calders et al., 2015; Tansey et al., 2009).

Individual trees within a diameter of 12.6 m from the central position were then marked in the complete point cloud of each plot. All identified trees were then extracted manually into individual tree point clouds. Most important for the manual extraction were the stem and an approximate crown as far as identifiable (Figure 8).

For the DBH extraction a circle was fitted to the point cloud at 1.3 m above the lowest tree point of the tree. In order to have sufficient points for the circle fitting the points from 1.27 m to 1.33 m where projected on a plane as in Tansey et al. (2009).

Two approaches for the circle fitting were tested. One was the least square adjustment, where the DBH resulted from the best fitting circle diameter minimizing through iterations the residuals from the circle to the points and implemented by Brown (2007). The other method used an approach of circle fitting by minimizes the sum of squared radial deviations as implemented by Bucher (2004).

Since the method used was originally used in an undergrowth-free and low branch-poor stand (Tansey et al. 2009), and many of the plots in the research area actually did have a considerable amount of undergrowth and low branches large overestimations were expected for some trees.

To counter the effect of overestimation the resulting DBH values were tested for outliers. The resulting DBH values were compared with the field measurements and values with a deviation higher than 20% were flagged. These outliers occurred mainly due to branches at the measuring height. To exclude the points of these branches and retain only the points belonging to the stem 20% of the outmost points of the flagged tree slices were removed and the DBH values were recalculated as in the previous steps. This procedure was repeated 5 times or until the deviations lay below 20% as compared to the field measurements.

The height was estimated by determining the highest and lowest point from the extracted tree point cloud and measure the distance between these two points.

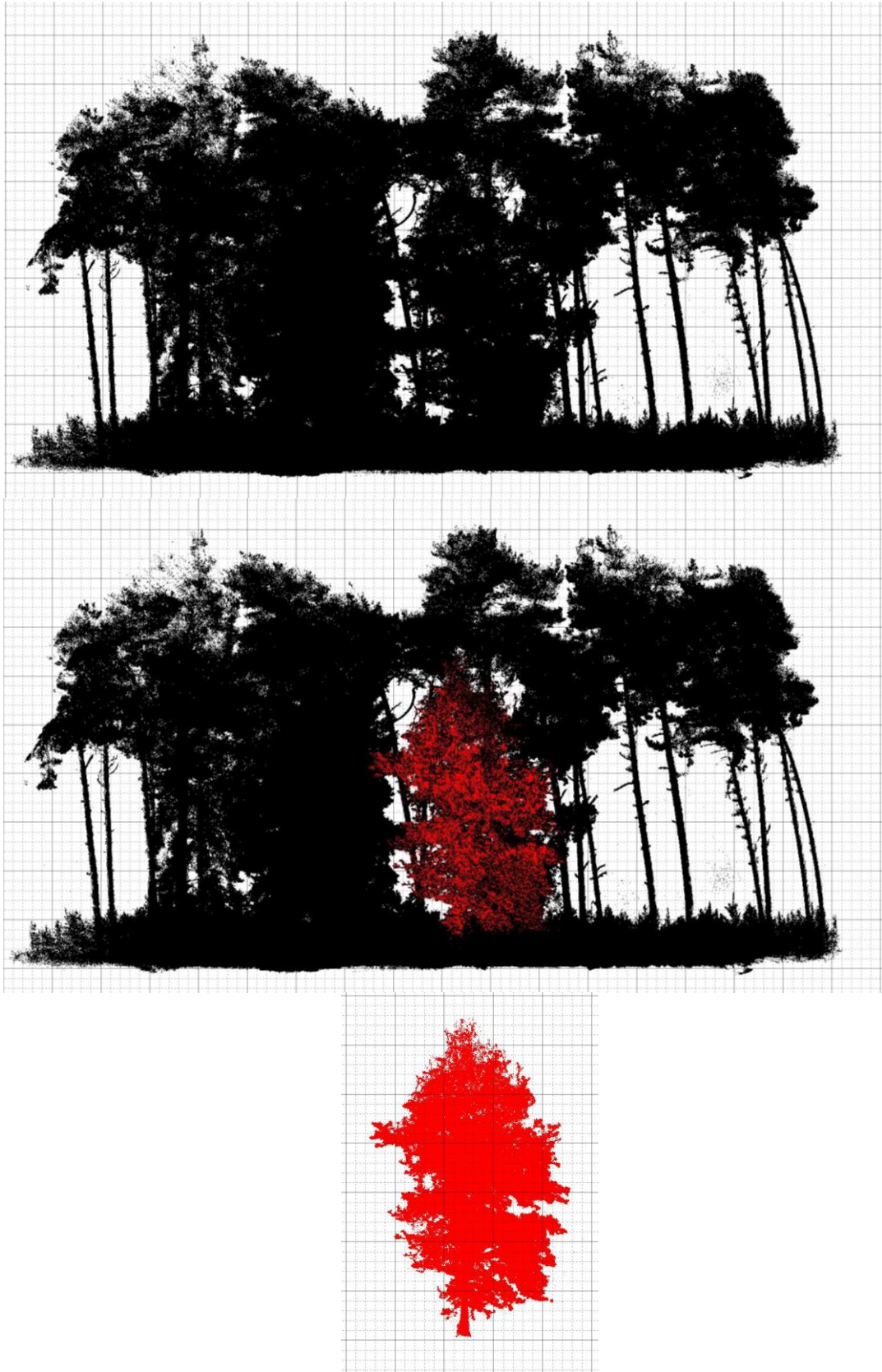


Figure 8: Upper figure: plot point cloud as obtained by combination of all five TLS plot scans (cropped just to include immediate plot surroundings). Middle figure: plot point cloud as above with marked individual tree as manually identified. Lower figure: isolated individual tree point cloud.

2.3. Data analysis

In Figure 9 the general steps of the analysis of the research questions 1 – 3 are shown. The analysis steps for the 4th research question are visualized in Figure 10.

For all analysis steps a confidence level of 95 % ($\alpha = 0.05$) was used.

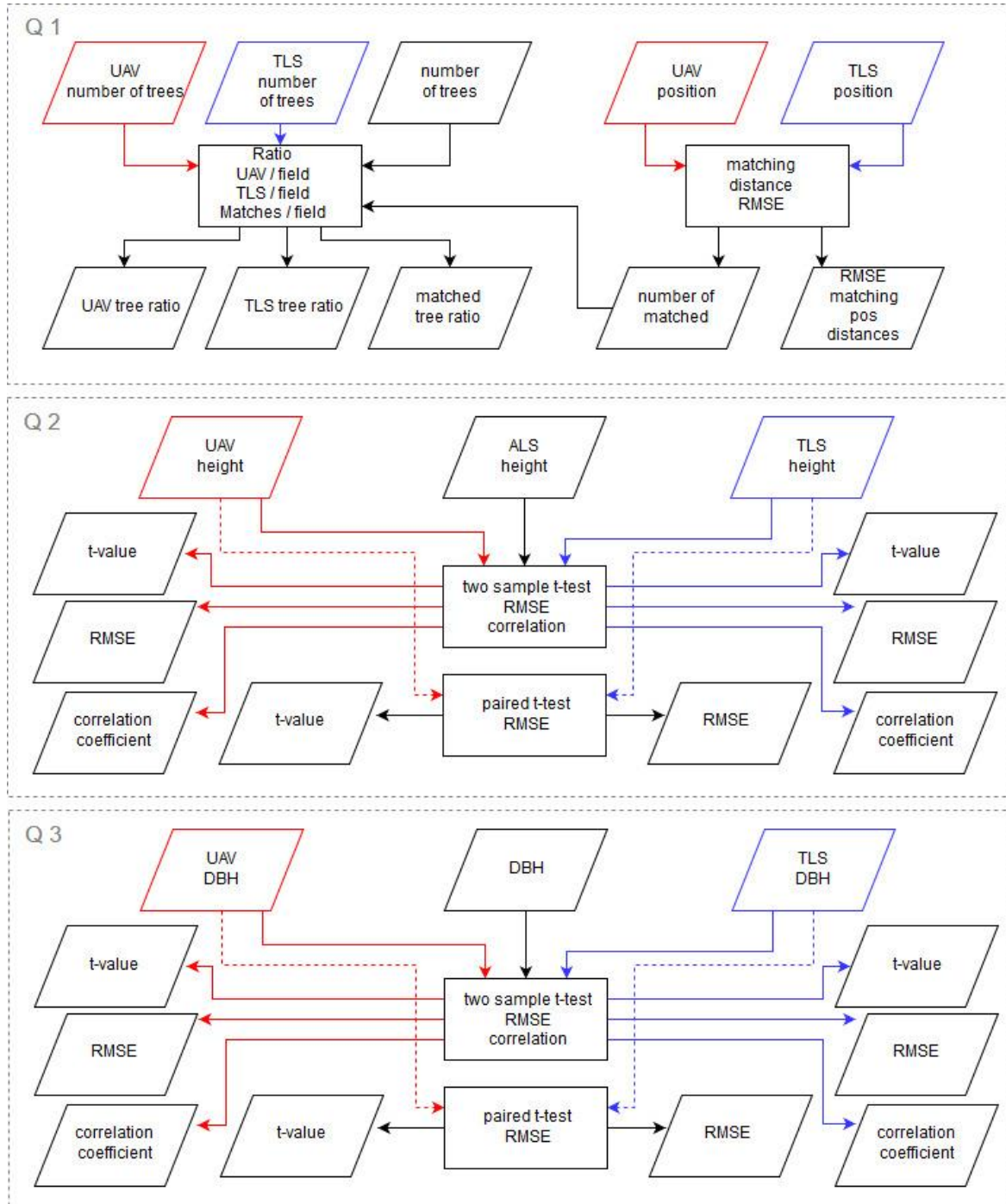


Figure 9: Data analysis steps for research question 1- 3 (Q 1-3). Red lines indicate UAV data input and output regarding only UAV and reference data comparisons, blue lines are assigned to respective TLS regarding analysis steps, black lines show reference data input and UAV and TLS comparative output.

1. *Does processing of the UAV and TLS data lead to the expected raw data for the analysis?*

- *Can all trees observed in the field be distinguished in the processed TLS data?*

The number of trees observed in the field was compared to the number of trees that could be extracted from the TLS data set. The Ratio of TLS trees to field observations was calculated.

- *Does the number of trees detected from the UAV data coincide with the number of trees observed in the field?*

A spatial overlay of the sampling plot areas and the crown centre points was performed to extract the number of UAV trees. The Ratio of UAV trees to field observations was calculated.

- *Do the positions of trees from the TLS and the UAV data sets coincide?*

For the position of the TLS trees the distinguishable trees in a point cloud were compared to the tree positions on the photos that were taken during the TLS scans. These positions were marked and their coordinates as point features exported.

For the identification of UAV derived trees with their TLS counterpart the UAV tree crown centre points were compared with the TLS tree point positions in ArcGIS.

Based on a closest neighbour approach the UAV centre point positions were matched to the TLS positions. When one TLS position was the closest match for more than one UAV position only the closest UAV position was matched. To avoid unrealistic identifications the matching was also confined to a radius of 5 m that seemed reasonable in the context of the sampling plots.

UAV tree positions that could not be matched were marked as “no match” as well as those TLS trees that could not be identified in the UAV data. All trees that were marked as “no match” were excluded from further analysis steps.

The positional deviations of the matched UAV and TLS trees were calculated with a point distance approach from TLS to UAV tree locations.

2. *Is there a significant difference between the UAV derived height values, TLS derived height values and the ALS reference height values?*

For the height derived from the UAV and TLS data over the reference data from the ALS and the UAV over TLS height the root mean square error (RMSE) was calculated.

The RMSE was calculated after the formula as noted by Barnston & Barnston (1992):

$$RMSE_{f_r} = \sqrt{\sum_{i=1}^n (x_{f_i} - x_{r_i})^2 / n}$$

Where

n = sample size

f = the height or DBH values derived from the UAV or TLS data

r = the reference height or DBH values from the ALS data or field measurements

- *Is there a significant difference between the UAV extracted height and the height from the canopy height model derived from ALS?*

The mean height per plot and its standard deviation was calculated from both UAV and ALS height values as well as the RMSE of UAV to ALS height values.

A two-sample t-test at confidence level $\alpha=0.05$ with unknown population standard deviation was done to establish if the mean of the UAV height values was significantly different from that of the ALS.

- *Is there a significant difference between the TLS derived height values and the height from the canopy height model derived from ALS?*

The mean height per plot and its standard deviation was calculated from both TLS and ALS height values as well as the RMSE of TLS to ALS height values.

A two-sample t-test at confidence level $\alpha=0.05$ with unknown population standard deviation was done to establish if the mean of the TLS height values was significantly different from that of the ALS.

- *Is there a significant difference between the TLS derived height values and the height values derived from the UAV data?*

The mean height per plot and its standard deviation was calculated from both UAV and ALS height values as well as the RMSE of UAV to TLS height values.

A paired t-test at confidence level $\alpha=0.05$ with unknown population standard deviation was done to establish if the mean of the UAV height values was significantly different from that of the TLS.

3. *Is there a significant difference between the UAV derived DBH values, TLS derived DBH values and the DBH values from the field measurements?*
 - *Is there a significant difference between the DBH estimated from the CPA measured from the UAV data set and the field measured DBH?*

The mean DBH per plot and its standard deviation was calculated from both UAV and field measured values as well as the RMSE of UAV to field measured DBH values.

A two-sample t-test at confidence level $\alpha=0.05$ with unknown population standard deviation was done to establish if the mean of the UAV DBH values was significantly different from that of the field measurements.

- *Is there a significant difference between the DBH estimated from the CPA measured from the UAV data set and the field measured DBH?*

The mean DBH per plot and its standard deviation was calculated from both TLS and field measured values as well as the RMSE of TLS to field measured DBH values.

A two-sample t-test at confidence level $\alpha=0.05$ with unknown population standard deviation was done to establish if the mean of the TLS DBH values was significantly different from that of the field measurements.

- *Is there a significant difference between the DBH estimated from the CPA measured from the UAV data set and the TLS derived DBH?*

The mean DBH per plot and its standard deviation was calculated from both UAV and TLS values as well as the RMSE of UAV to TLS DBH values.

A paired t-test at confidence level $\alpha=0.05$ with unknown population standard deviation was done to establish if the mean of the UAV DBH values was significantly different from that of the TLS.

Q 4

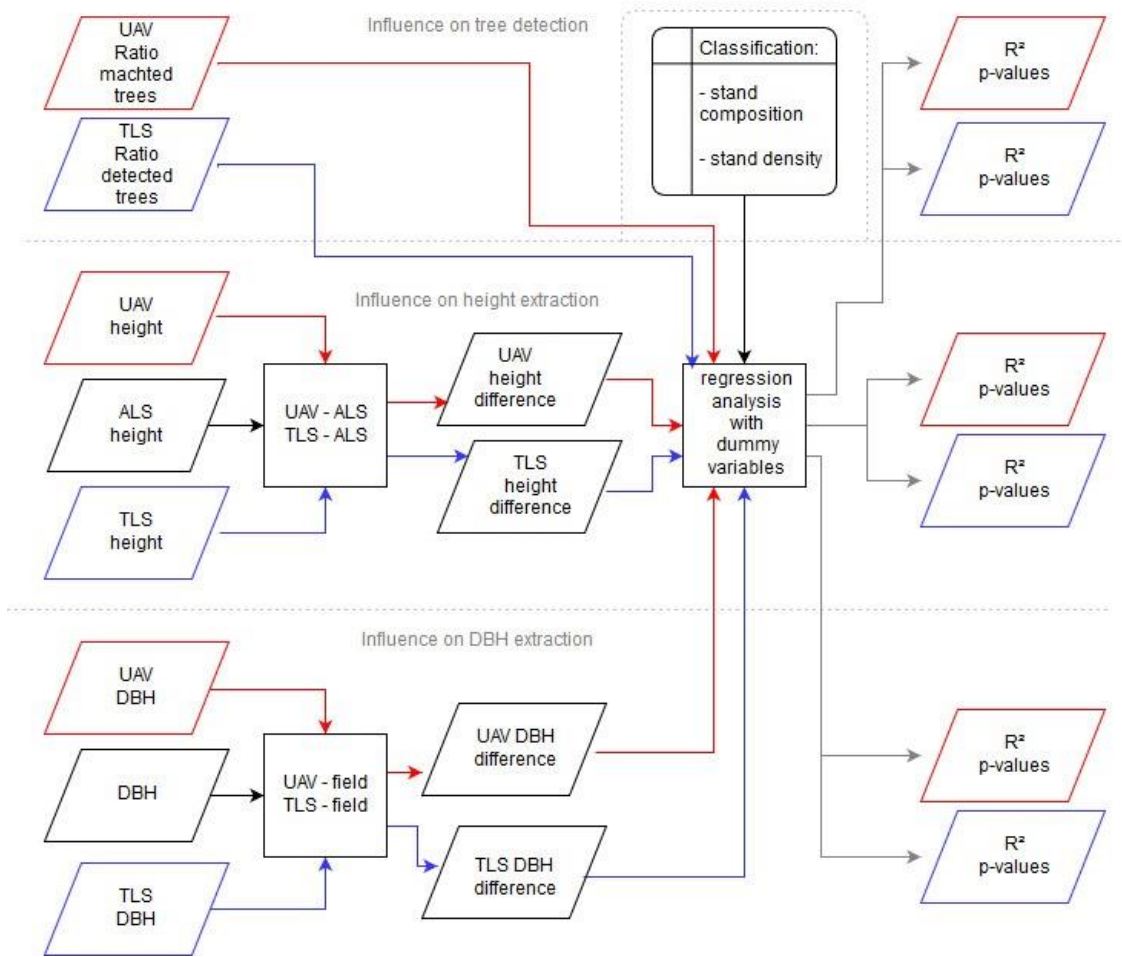


Figure 10: Analysis steps for Research question 4. Blue marks the TLS data input and relevant output, red marks the UAV data steps, black lines show reference data input

4. Do forest type and structure influence the tree and parameter (height and DBH) extraction from UAV and TLS data?

To determine whether the stand composition and stand density had a significant influence on the completeness of tree detection and the accuracy of parameter extraction from both the UAV and the TLS data a linear regression analysis was performed using dummy variables for the stand composition and density. For the dummy variables, the stand composition and stand density were classified into different categories.

The forest composition was divided into three categories: deciduous, mixed and coniferous. These classifications were assigned plot based and per the species occurrence within each plot. For the classification of deciduous or coniferous stand composition, the trees of the plot needed to be 80% or more deciduous or coniferous species respectively. Below this threshold value the stand was defined to be a mixed composition (Table 1).

For the stand density, the number of trees per ha was also divided into three classes. Low density, less than 300 trees per ha; medium density of 300 – 500 trees per ha and more than 500 trees per ha is high density (Table 1).

Table 1: Classification criteria for the stand composition and stand density

Stand composition	Deciduous	Mixed	Coniferous
	$\geq 80\%$ Deciduous trees	$< 80\%$ deciduous and coniferous trees	$\geq 80\%$ Coniferous trees
Stand density	High	Medium	Low
	> 500 trees per ha	300 – 500 trees per ha	< 300 trees per ha

- Does the **stand composition** influence the **tree detection** from the TLS and UAV data set?
- Does the forest **stand density** influence the **tree detection** from the TLS and UAV data set?

For the analysis of the influence of stand composition and density on the completeness of the tree detection from UAV and TLS data, the percentage of extracted trees from the TLS data set and the percentage of matched trees from the UAV data set per plot was examined as a function of stand composition and stand density. Three linear regression models were fit based on the dummy coded stand composition, stand density and stand composition and density. The base model was built as a function of the coniferous composition class and the low-density class.

- Does the **stand composition** influence the tree **height** extraction from the TLS and UAV data set?
- Does the forest **stand density** influence the tree **height** extraction from the TLS and UAV data set?

For the analysis of the influence of stand composition and density on the height extraction error from UAV and TLS data, the difference between UAV and ALS height values, TLS and ALS height values and UAV and TLS height values was examined as a function of stand composition and stand density. Three linear regression models were fit based on the dummy coded stand composition, stand density and stand composition and density. The base model was built as a function of the coniferous composition class and the low-density class.

- Does the **stand composition** influence the **DBH** extraction from the TLS and UAV data set?
- Does the forest **stand density** influence the **DBH** extraction from the TLS and UAV data set?

For the analysis of the influence of stand composition and density on the DBH extraction error from UAV and TLS data, the difference between UAV and field DBH values, TLS and field DBH values and UAV and TLS DBH values was examined as a function of stand composition and stand density. Three linear regression models were fit based on the dummy coded stand composition, stand density and stand composition and density. The base model was built as a function of the coniferous composition class and the low-density class.

3. RESULTS

3.1. Field measurements

During the field measurements 18 plots were established and all trees with a diameter equal or higher than 10 cm in diameter. In total 458 trees were measured. The mean number of trees per plot was about 25 and 26 trees varying from 6 to 41 trees per plot. Four of the sampling plots were excluded from the analysis since the UAV images for the area they were located could not be properly processed (see 3.2 UAV image processing). In the 14 remaining plots, there were 341 trees with a mean DBH of 27.7 cm varying from 10 cm to 104 cm (Table 2 and Figure 11).

Table 2: Descriptive statistics of data acquisition and processing for all sampling plots included in the analysis

Forest type	Number of measured trees	Mean # of trees per plot	Mean of trees per ha	Mean DBH
All	341	25.05	500 stems/ha	23.46 cm
Deciduous	222	31.75	635 stems/ha	22.60 cm
Coniferous	37	9.25	185 stems/ha	34.01 cm
Mixed	82	27.33	547 stems/ha	24.86 cm

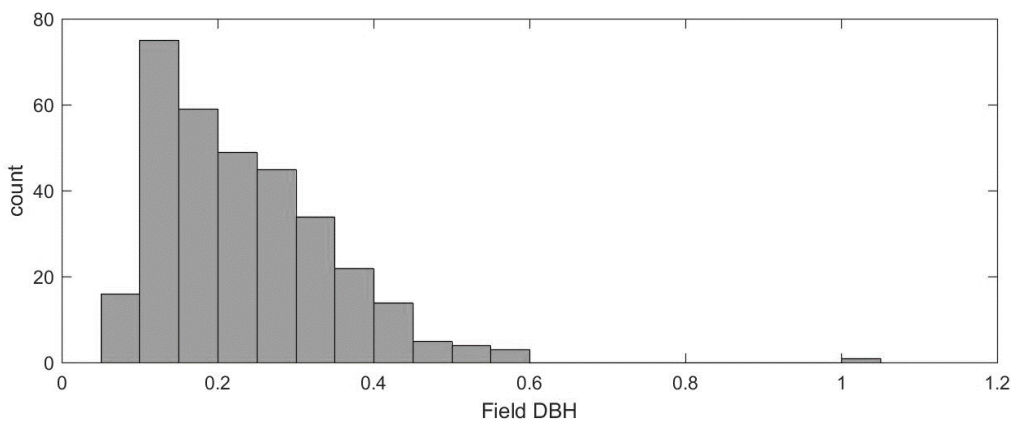


Figure 11: Distribution of field measured DBH (in meter) (including only the 14 sampling plots used in the analysis)

3.2. UAV image processing

The UAV data acquisition was done in 5 flights over the research area. The image calibration and SfM process was performed for each flight separately. Table 3 shows the results of image calibration. For 3 flights the calibration of images was mostly complete (2, 3, 4 in Table 3). For one flight (flight 1 in Table 3) a cluster of images in the centre area could not be calibrated. Since the resulting hole in the point cloud was not immediately over a sampling plot location and the resulting data could be used for further processing. The calibration of the last flight 5 images (flight 5 in Table 3) was not successful. Almost 25% of the images were not calibrated and those images that were calibrated, were tilted and positioned erratically (Figure 12). The flight area was excluded from further processing as well as the 131 trees in the four sampling plots in this area.

Table 3: Calibration results for UAV image calibration process: number of images, number and percentage of calibrated images and the root mean squared error (RMSE) of the geo-referencing with the ground control points (GCPs). For flight area 5 (marked red) no RMSE error was calculated since no satisfactory image calibration was reached.

Flight area	Total number images	Calibrated images		RMSE to GCPs (m)
1	154	142	92.2 %	0.001
2	170	168	98.8 %	0.016
3	176	176	100 %	0.005
4	232	232	100 %	0.013
5	204	159	77.4 %	-

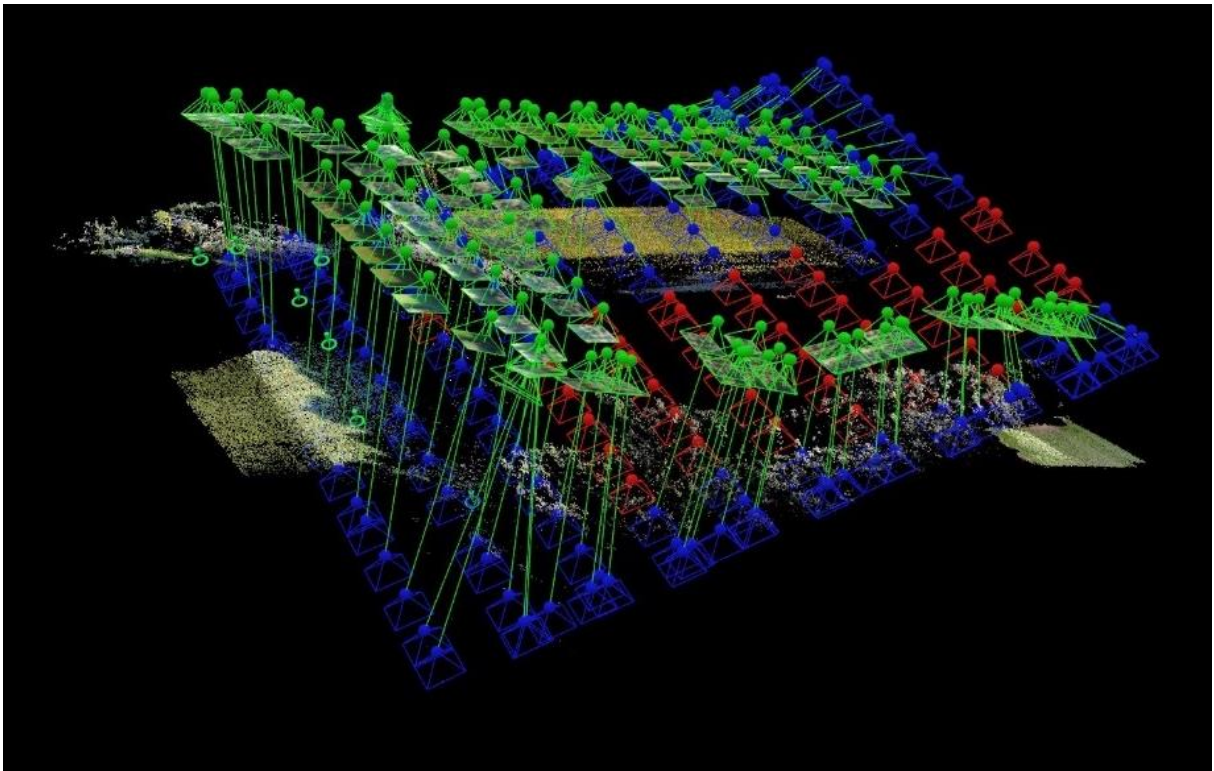


Figure 12: Results of the image calibration attempt of the 5th UAV flight. Blue pyramids represent the recorded UAV GPS position when the picture was taken. Green pyramids show the calculated position after the Pix4D calibration

(with additional manual tie points (green circles with pin) and GCPs (blue circles with pin)). Red pyramids signal images that could not be calibrated.

The linear model used for the DBH calculations from the UAV data was based on both CPA and height values:

$$DBH_{UAV_i} = 0.02943 + 0.00433 * CPA_i + 0.00727 * height_i$$

adjusted R²= 0.483

P-values: CPA = 0.0000366165, height=0.117997044

Although the p-value for the height parameter in the regression model did not fall within the range of the 95% confidence level chosen as threshold value, the overall model fit was better than the alternative model based only on the CPA which was a slightly lower fit (R²=0.477).

3.3. TLS data processing

The DBH estimations without any applied filter for low branches and undergrowth resulted in overestimations for several trees (Figure 13).

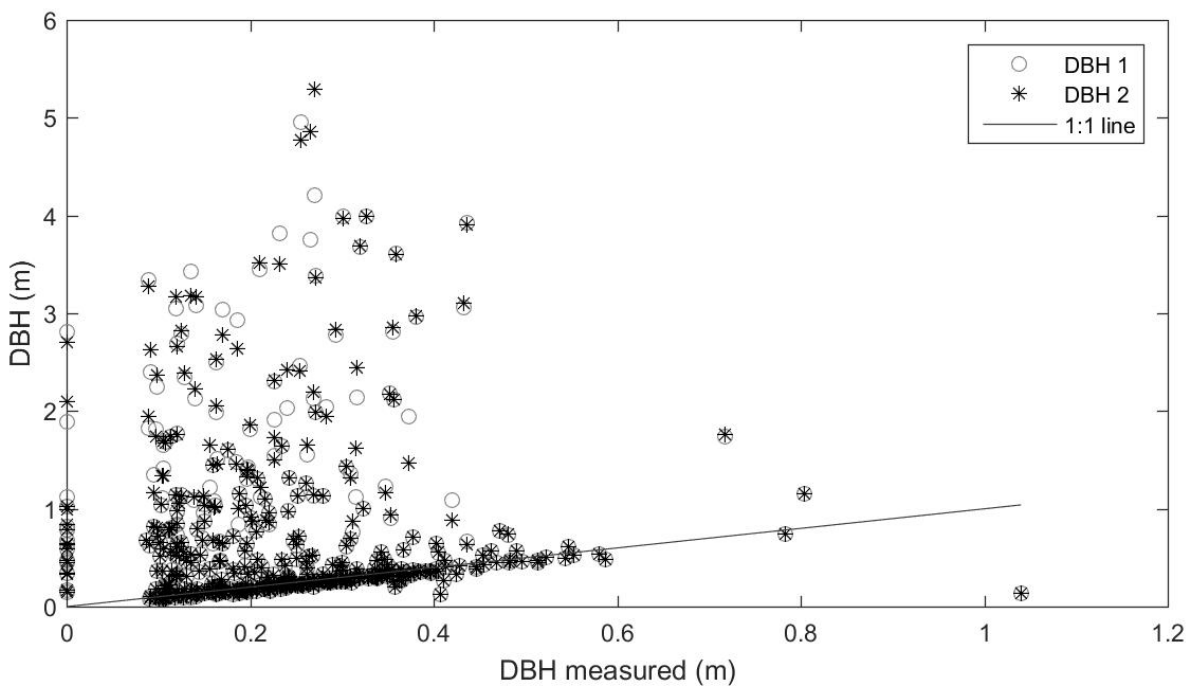


Figure 13: Results of two DBH calculation methods (blue circles and red stars) without any filtering for the TLS data in relation to the field measured DBH (yellow 1:1 line).

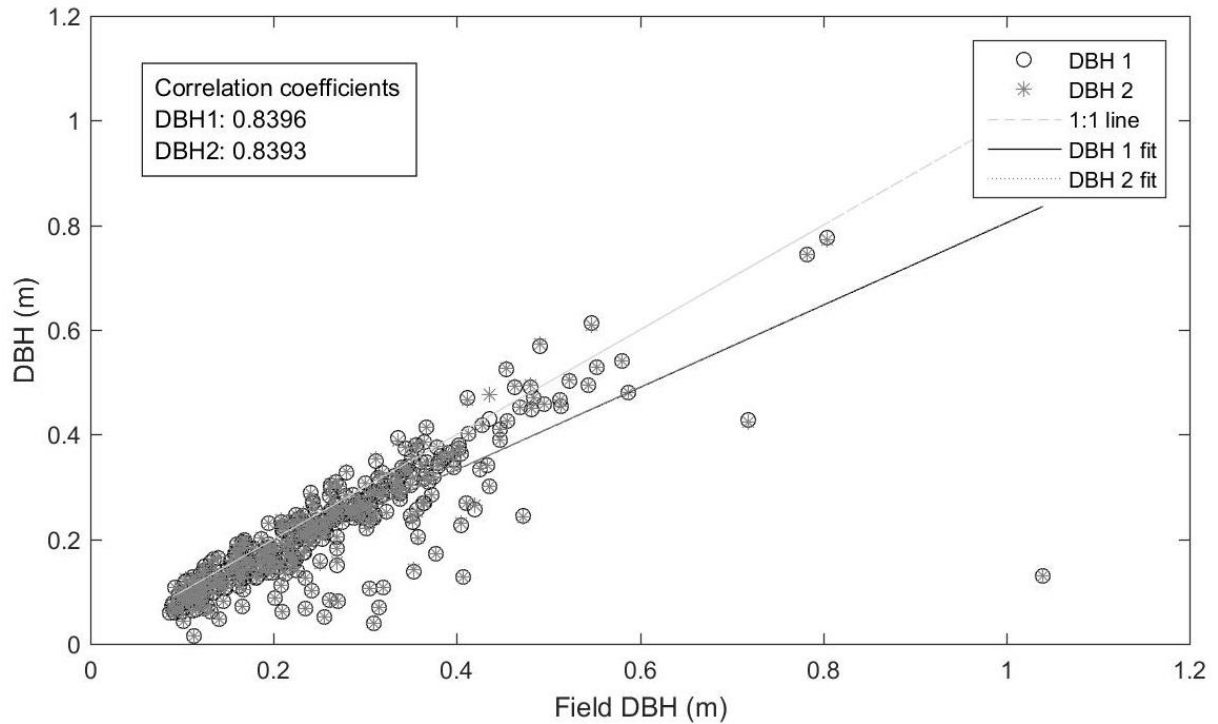


Figure 14: Results of the both DBH calculation methods (blue circles and red stars) for the TLS data in relation to the field measured DBH (yellow 1:1 line) after excluding calculated TLS DBH values that had more than + 20 % deviations from the Field values. The blue and green line show the respective polynomial fit of DBH 1 and DBH 2. The Correlation coefficient of each set to the Field DBH is displayed in the upper left corner.

In Figure 14 the results from both DBH calculation methods from the TLS data are displayed as well as their polynomial fits and the correlation coefficient for each method's results. Since values higher than 1.2 times the Field DBH were excluded from the polynomial fits (Figure 16) the results are more strongly influenced by DBH values that are lower than the measured DBH values. Based on the slightly better correlation of the DBH1 method the results of this method were used as DBH estimation from the TLS data set for the analysis. Both estimation methods seem to generally underestimate the DBH as compared to the field results. This bias is also partly a result from the implemented filtering procedure since some of the results clearly underestimate the DBH compared to the field measurements (Figure 15). Several of the values estimated from a resampled point cloud, particularly for smaller DBH values, are considerably smaller than the measured DBH.

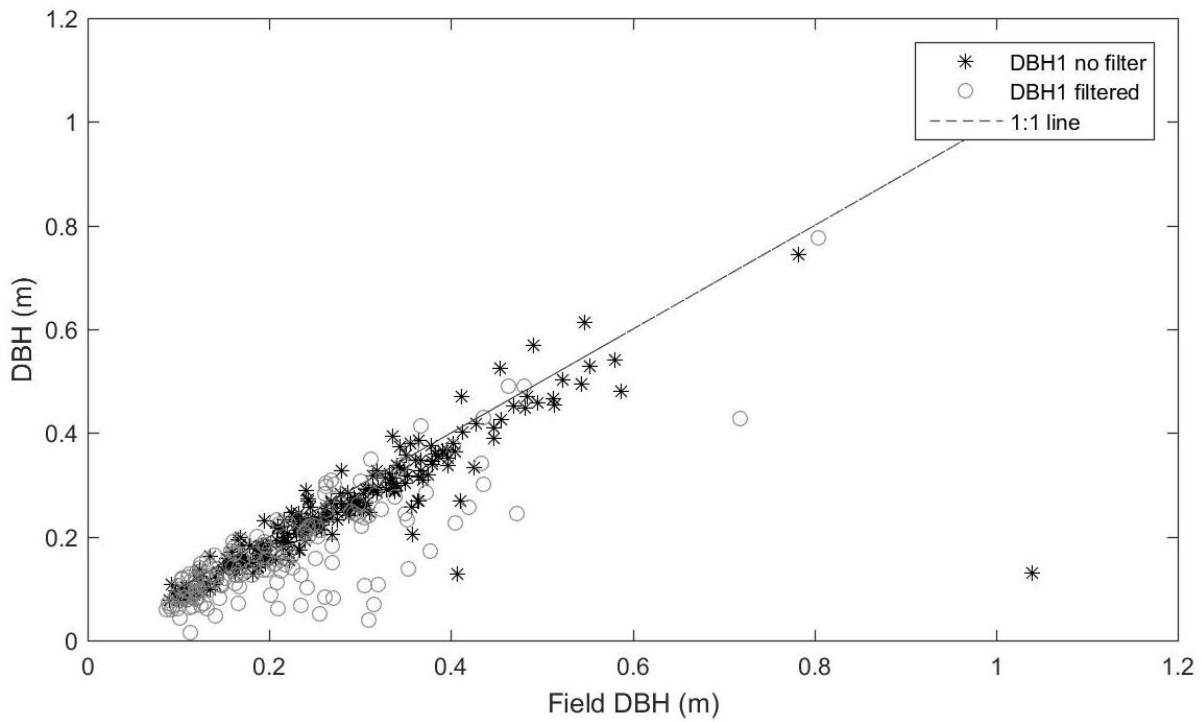


Figure 15: TLS DBH values calculated after the first method after running through filtering to eliminate noise. Stars (black) show the DBH results of trees that were not filtered while the circles (grey) indicate those values obtained after filtering out the outer 20 % of the stem point cloud.

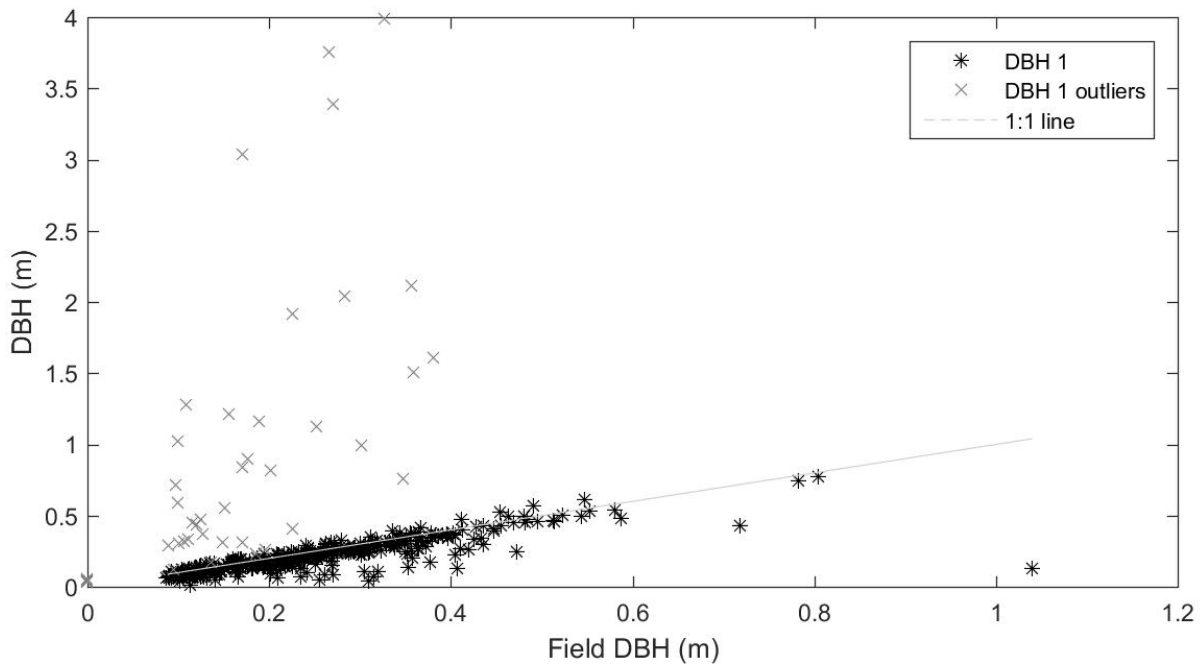


Figure 16: The DBH values as calculated from the TLS tree data with the first calculation method. The crosses mark those DBH values that have been identified as outliers and were excluded from further analysis.

3.4. UAV and TLS data processing and tree detection

The results of the tree detection and matching process follow the order of the sub points of the first research question.

3.4.1. TLS tree detection

From the TLS data 324 trees could be extracted within the sampling area. They represented 95% of all trees that were counted during the field measurements. Table 4 shows the plot-wise results.

3.4.2. UAV tree delineation

The total number of delineated trees derived from the UAV data was of 298 which corresponded to 87.4% of the number of trees observed during the field measurements (Table 4).

3.4.3. Tree position matching

Table 4 shows the number of identified trees from the field, the TLS processing and the UAV image process as well as the number of matched trees per plot and the mean distance between the respective positions.

Table 4: Number of trees in remaining sampling plots, field measured (Field), TLS extracted (TLS and number of tree tops/crowns identified from the UAV data (UAV) in the plot area (crowns) and the number of trees that were successfully matched (matched) to the field and TLS positions as well as the mean distance of matched UAV tree positions to the TLS positions.

plot	Field	TLS		UAV			Mean distance of UAV to TLS
				crowns	matched		
0908_1	15	13	86,7 %	21	9	60 %	3.75 m
0912_1	29	26	89.7 %	20	18	62.1 %	3.25 m
0912_2	38	36	94.7 %	50	23	60.5 %	3.96 m
0922_1	10	10	100 %	11	7	70 %	1.69 m
0922_2	6	6	100 %	7	5	83.3 %	1.93 m
0923_1	7	7	100 %	9	7	100 %	2.52 m
0923_2	32	32	100 %	24	20	62.5 %	3.21 m
0923_3	29	27	93.1 %	29	14	48.3 %	3.20 m
0924_1	16	16	100 %	13	12	75 %	2.94 m
0924_2	41	37	90.2 %	36	22	53.7 %	3.60 m
0926_1	34	34	100 %	21	14	41.2 %	2.58 m
0926_2	39	35	89.7 %	22	15	38.5 %	2.84 m
1024_1	13	13	100 %	17	8	61.5 %	3.30 m
1026_1	32	32	100 %	18	18	56.3 %	2.91 m
total	341	324	95.0 %	298	192	56.3 %	2.98 m

3.5. Tree height extraction and accuracy

The results for the comparison of tree heights from UAV, TLS and ALS reference values are shown in the order of the sub points of the second research question.

3.5.1. UAV to ALS

For the comparison of height values from UAV data and the ALS reference data a RMSE of 7.652 m was calculated. The mean and standard deviation of height values per plot can be seen in Table 5.

The results of the two-sample t-test show that the values are statistically significantly different. Figure 17 shows the distribution of UAV trees height values over the ALS trees height values and their correlation value.

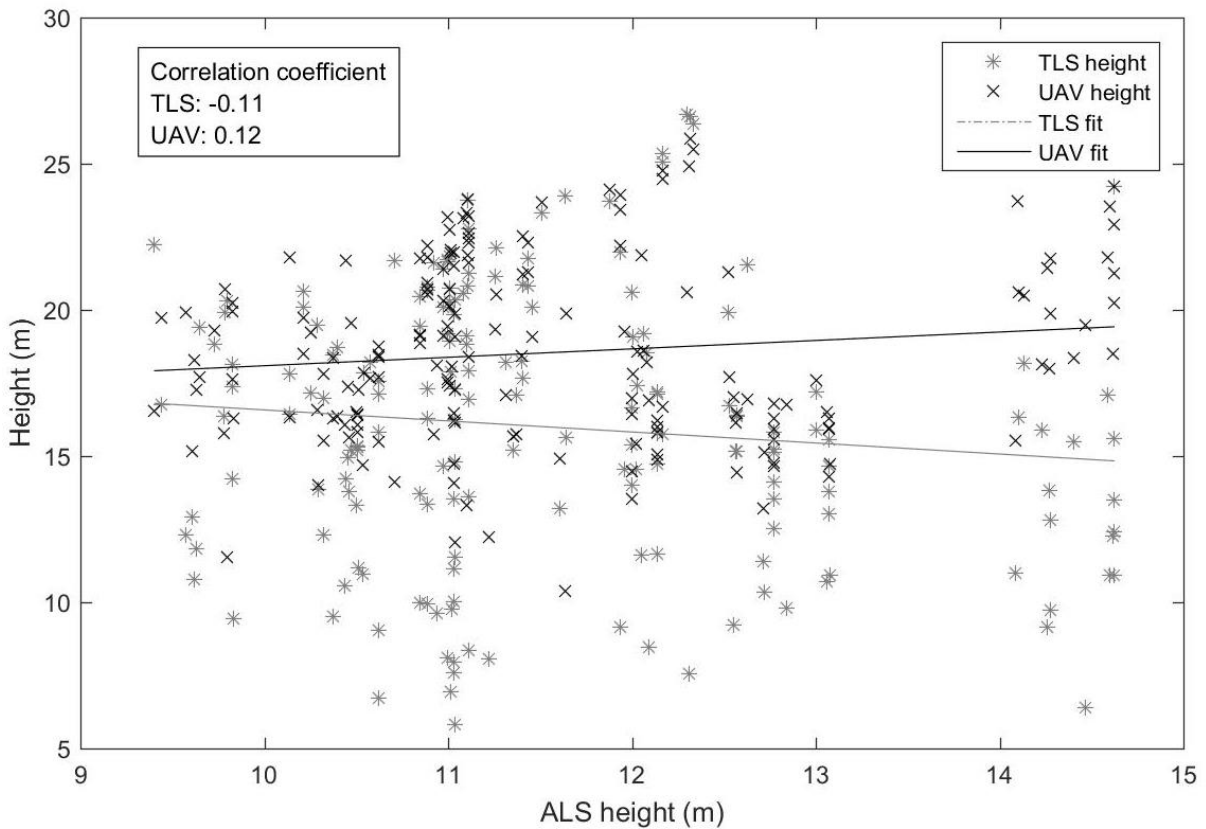


Figure 17: TLS (grey stars and line) and UAV (black crosses and line) height values for the matched trees compared to the ALS derived height values and the correlation values.

3.5.2. TLS to ALS

For the comparison of height values from TLS data and the ALS reference data a RMSE of 6.587 m was calculated. The mean and standard deviation of height values per plot can be seen in Table 5.

The results of the two-sample t-test show that the values are statistically significantly different. Figure 17 shows the distribution of TLS trees height values compared to the ALS trees height values and their correlation value.

3.5.3. UAV to TLS

The RMSE between UAV and TLS height values was 5.460 m. The mean and standard deviation of the differences per plot can be seen in

Table 6.

The height values from both data sets have not been found to be significantly different. The distribution of UAV trees height values over TLS trees height values and their correlation can be seen in Figure 18.

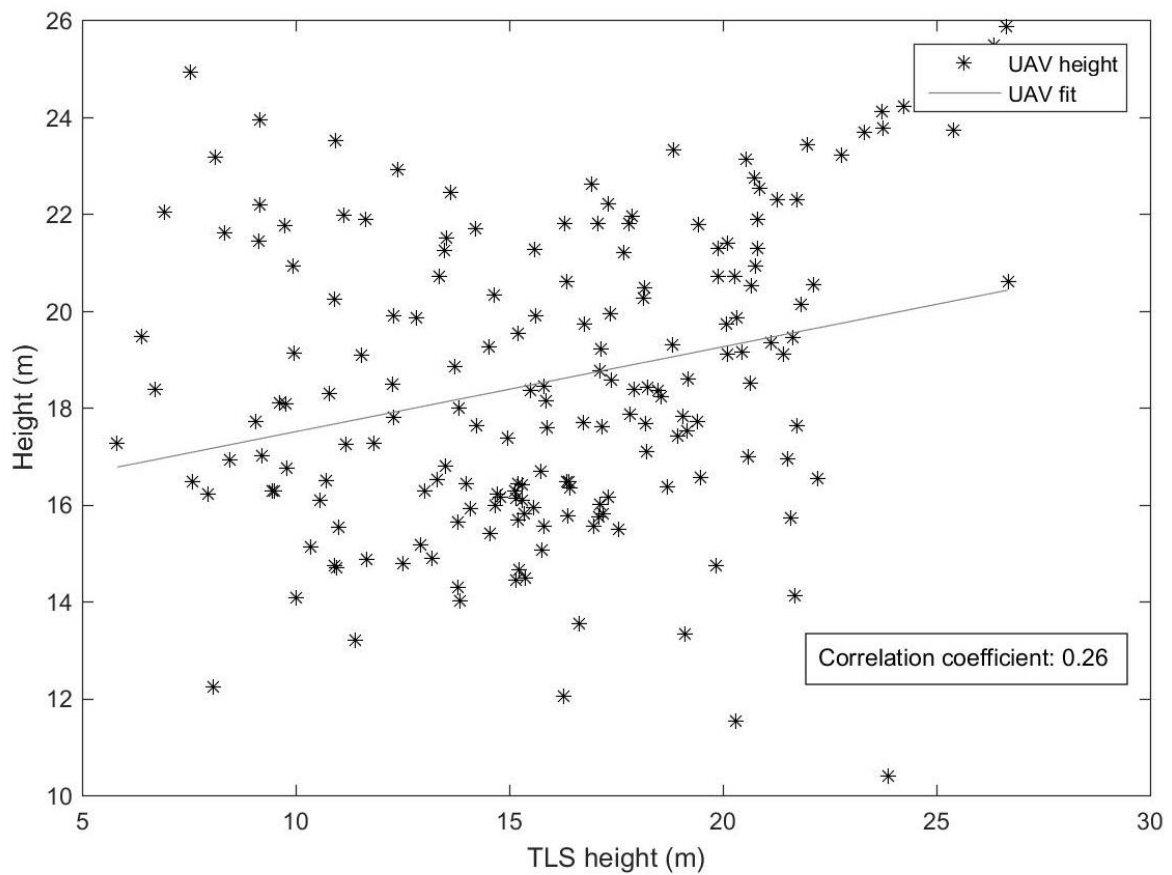


Figure 18: UAV height values (black stars and grey trend line) over the TLS height values for the matched trees and the correlation coefficient.

Table 5: Plot-wise UAV, TLS and ALS height means and standards deviations of matched trees

plot	TLS		UAV		ALS	
	Mean	Std	Mean	Std	Mean diff	Std
total	15.98 m	4.60 m	18.55 m	3.072 m	11.59 m	1.30 m
0908_1	17.676	3.855	21.002	0.703	10.928	0.059
0912_1	15.749	3.538	18.674	2.032	9.799	0.301
0912_2	14.255	4.119	17.186	1.363	10.599	0.266
0922_1	16.444	3.980	15.668	2.722	11.522	0.480
0922_2	21.539	1.513	15.485	5.068	11.008	0.763
0923_1	20.216	1.773	17.454	2.259	10.933	0.318
0923_2	13.916	1.928	15.522	0.958	12.779	0.265
0923_3	13.706	5.089	18.019	2.140	11.891	0.709
0924_1	19.954	7.577	23.559	1.970	12.062	0.248
0924_2	16.370	5.351	21.214	2.417	11.074	0.212
0926_1	14.837	3.820	19.265	2.671	13.291	1.320
0926_2	15.058	5.450	20.660	2.569	14.427	0.226
1024_1	18.482	4.294	19.593	1.071	10.758	0.363
1026_1	15.163	1.540	15.942	0.904	11.471	0.924

Table 6: Plot-wise mean and standard deviation of height differences between TLS and ALS, UAV and ALS, UAV and TLS

plot	TLS to ALS		UAV to ALS		UAV to TLS	
	Mean	Std	Mean	Std	Mean diff	Std
All	4.386	4.928	6.957	3.195	2.571 m	4.830 m
0908_1	6.748	3.827	10.073	0.735	3.326	4.052
0912_1	5.950	3.581	8.874	1.900	2.924	3.610
0912_2	3.657	4.204	6.587	1.297	2.930	4.411
0922_1	4.922	3.874	4.146	2.535	-0.776	2.497
0922_2	10.531	1.298	4.476	4.797	-6.055	5.786
0923_1	9.283	1.573	6.520	2.362	-2.762	2.782
0923_2	1.136	2.032	2.743	0.988	1.606	1.836
0923_3	1.815	4.932	6.129	2.172	4.313	5.233
0924_1	7.892	7.538	11.497	1.922	3.605	7.368
0924_2	5.295	5.284	10.140	2.371	4.845	5.015
0926_1	1.546	4.791	5.974	2.360	4.427	5.365
0926_2	0.631	5.491	6.233	2.482	5.602	4.481
1024_1	7.724	4.328	8.835	1.007	1.111	4.141
1026_1	3.692	1.481	4.471	1.017	0.780	1.351

3.6. DBH extraction and accuracy

The results for the comparison of DBH values from UAV, TLS and field measurements are shown in the order of the sub points of the third research question.

3.6.1. UAV to field

For the comparison of estimated DBH values from UAV data and the field measurements a RMSE of 0.124 m was calculated. The mean and standard deviation of DBH values per plot can be seen in Table 7.

The results of the two-sample t-test show that the UAV DBH values are not significantly different from the field measurements. Figure 19 shows the distribution of UAV derived DBH values over the field measurements and their correlation value can be observed.

3.6.2. TLS to field

For the comparison of TLS DBH values and the field measurements a RMSE of 0.334 m was calculated. After the omission of the 5 most extreme outliers the new RMSE value was 0.079 m. The mean and standard deviation of DBH values per plot can be seen in Table 7: .

The results of the two-sample t-test show that the TLS DBH values are not significantly different from the field measurements. Figure 19 shows the distribution of TLS DBH values over the field measurements and their correlation value can be observed too.

3.6.3. UAV to TLS

The RMSE between UAV and TLS DBH values was 0.128 m. The mean and standard deviation of the differences per plot can be seen in Table 8.

The height values from both data sets have not been found to be significantly different.

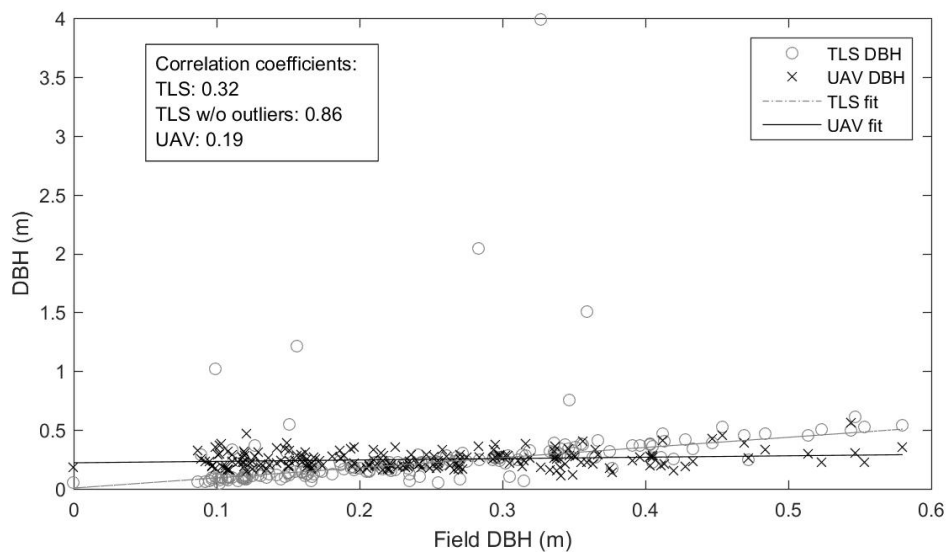


Figure 19: TLS DBH values (grey circles and dashed line) and UAV DBH values (black crosses and continuous line) for the matched trees over the field measurements of DBH. The correlation coefficient for the TLS values was calculated with (TLS) and without the five most prominent outliers ((TLS w/o outliers, outlier DBH values > 1 m).

Table 7: Plot-wise UAV, TLS and field measured DBH (and CPA for UAV) means and standards deviations of matched trees

plot	TLS		UAV				Field	
	Mean	Std	CPA		DBH		Mean	std
			Mean	Std	Mean	std		
total	0.269 m	0.355 m	19.938 m²	14.305 m²	0.250 m	0.072 m	0.244 m	0.115 m
0908_1	0.243	0.118	25.112	12.159	0.291	0.053	0.306	0.099
0912_1	0.222	0.121	19.261	12.263	0.248	0.057	0.256	0.120
0912_2	0.163	0.067	8.525	5.615	0.191	0.028	0.184	0.088
0922_1	0.790	1.411	23.889	13.105	0.247	0.073	0.296	0.025
0922_2	0.296	0.079	11.832	15.422	0.193	0.103	0.367	0.024
0923_1	0.260	0.094	14.481	10.438	0.219	0.057	0.363	0.039
0923_2	0.311	0.445	19.846	15.241	0.228	0.066	0.224	0.065
0923_3	0.215	0.173	17.509	12.207	0.236	0.059	0.233	0.159
0924_1	0.346	0.156	32.523	23.310	0.341	0.108	0.346	0.168
0924_2	0.181	0.097	14.478	8.873	0.246	0.046	0.194	0.096
0926_1	0.174	0.097	24.827	11.457	0.277	0.061	0.213	0.092
0926_2	0.226	0.170	24.545	13.091	0.286	0.069	0.179	0.125
1024_1	0.569	0.499	26.518	15.073	0.287	0.067	0.306	0.094
1026_1	0.261	0.212	25.788	15.706	0.257	0.070	0.229	0.088

Table 8: Plot-wise mean and standard deviation of DBH differences between TLS and field measurements, UAV and measurements, UAV and TLS

plot	TLS to field measurements		UAV to field measurements		UAV to TLS	
	Mean (m)	Std (m)	Mean (m)	Std (m)	Mean(m)	Std (m)
total	0.025	0.337	0.007	0.124	-0.018	0.356
0908_1	-0.063	0.092	-0.016	0.112	0.048	0.112
0912_1	-0.034	0.039	-0.008	0.136	0.026	0.136
0912_2	-0.021	0.036	0.007	0.097	0.028	0.079
0922_1	0.494	1.397	-0.049	0.068	-0.543	1.440
0922_2	-0.071	0.083	-0.174	0.091	-0.103	0.123
0923_1	-0.103	0.093	-0.144	0.076	-0.041	0.111
0923_2	0.087	0.426	0.004	0.093	-0.083	0.414
0923_3	-0.018	0.037	0.003	0.166	0.022	0.177
0924_1	-0.001	0.064	-0.005	0.178	-0.004	0.162
0924_2	-0.013	0.055	0.052	0.092	0.066	0.090
0926_1	-0.039	0.030	0.064	0.128	0.103	0.129
0926_2	0.047	0.129	0.107	0.083	0.060	0.155
1024_1	0.263	0.522	-0.020	0.103	-0.283	0.524
1026_1	0.032	0.229	0.028	0.106	-0.004	0.189

3.7. Forest type and stand structure influence

Table 9: Number of matched trees per composition and density

Composition/density	Low	Medium	High	All
Coniferous	19	0	0	19
Mixed	8	26	12	46
Deciduous	0	26	93	119
All	27	52	105	184

The number of trees per composition and density class can be seen in Table 9. The highest number of trees were found in the density class high and the composition class deciduous. Deciduous class trees in high density stands represented over 50% of all matched trees.

The results of the linear regression analysis over the influence of stand composition and density on tree detection, height and DBH extraction accuracy are summarized in Table 10.

Table 10: Results of multiple linear regression analysis with dummy variables. Results displayed are adjusted R² (R² adj., light grey) and p-values for the variables. The variables were: for the stand composition, mixed (mix.) and deciduous (dec.) over the coniferous model; for the stand density, medium (med.) and high (high) over the low model. P-values higher than the chosen $\alpha=0.05$ are marked in dark grey (p-value > α)

R ² and p-values ->		Stand composition			Stand density		
		R ² adj.	Mix.	Dec.	R ² adj.	Med.	High
Tree det.	UAV	0.464	0.010	0.006	0.409	0.075	0.007
	TLS	0.046	0.148	0.208	0.229	0.034	0.173
	pos.	0.078	0.002	0.000	0.043	0.007	0.002
Height	UAV-ALS	0.076	0.000	0.035	0.145	0.000	0.938
	TLS-ALS	0.076	0.035	0.000	0.127	0.023	0.000
	UAV-TLS	0.139	0.000	0.000	0.127	0.000	0.000
DBH	UAV-field	0.110	0.000	0.000	0.114	0.003	0.000
	TLS-field	-0.001	0.213	0.186	0.023	0.015	0.037
	UAV-TLS	0.031	0.013	0.004	0.066	0.001	0.000

4. DISCUSSION

4.1. Data acquisition and processing

The acquisition and processing of both TLS and UAV data both represent different challenges because of sources for errors and inaccuracies.

4.1.1. TLS data acquisition and processing

The TLS data acquisition was relatively time consuming compared to the UAV image acquisition process. It was also restricted by the accessibility of the research area which limited the data acquisition in some cases and introduced a bias to the analysis. Certain forest types with too dense undergrowth vegetation could not be sampled with the TLS and were therefore not included in the direct comparison with the UAV. This biased the analysis since only relatively optimal TLS sampling areas were included while areas with unfavourable conditions for the TLS conditions were omitted. This should be considered when interpreting the results since it might have biased the TLS results towards a higher accuracy based on favourable sampling conditions.

The manual tree extraction from the TLS point clouds was time consuming and required subjective decisions. Though most trees measured in the field for reference could be identified in the TLS data (Table 4) the extraction of individual trees, especially the crowns, was hampered by several natural and data related factors. These factors made it difficult to recognize the belonging of certain objects or point groups to a tree and make the correct extraction of trees a very complex process (Figure 20 and Figure 21). Though the factor of occlusion has been tried to be minimized by the sampling design and number of scanning positions in plot it could not completely be avoided in all cases. Especially in more dense stands and in the tree crowns there was often partial occlusion by trees or branches in the line of sight of the scanner which lead to occlusion. This occlusion made the recognition of the continuity and connection of objects, such as branches, difficult and a question of subjective interpretation (Figure 20). The occurrence of “shadows”, points that seem to be shadowing areas behind a certain object without any surface they could have been reflected off, introduce another source of uncertainty in the extraction process (Figure 21). The free-floating points trailing behind objects and the occlusion effects by branches and foliage create a more scattered appearance of the point cloud. This combination of effects is particularly noticeable in the crown areas where it complicates the correct separation of crowns and the identification of tree tops.

In some cases, the separation and extraction of individual trees was also complicated by natural growth form of trees. Strongly intertwined trees and branches (Figure 20) made the manual separation time consuming and increased the probability of introducing errors by either including non-belonging objects or excluding belonging objects during the extraction of individual trees.

Due to the complexity of the task the automatic solution for the tree extraction is rather challenging. In many studies and for economic purposes the solutions for automatic tree recognition are limited to the stem detection and the DBH calculation (e.g. Olofsson, Holmgren, & Olsson, 2014). Nevertheless, several studies and researchers are investigating the possibilities of automatic tree extractions for example via an object based approach (Hackenberg et al. 2015). Although sometimes with relatively good results these studies were mostly done in relatively open stands with few intermingled crowns (Calders et al. 2015).



Figure 20: left: Occlusion of structures/objects (see red circles) make recognition of connected structures (e.g. branches) difficult. Right: Intertwined tree stems that cannot effectively be separated and create errors especially when measuring DBH.



Figure 21: The occurrence of “shadows” of points behind objects (see red circles) add to general complexity of structures and make the recognition of interconnected and separated objects as well as the recognition of finer structures difficult.

4.1.2. UAV data acquisition and processing

The UAV image acquisition was relatively fast compared to the TLS measurements. Apart from the flying time the flight planning and the preparation for the geo-referencing also went into the acquisition process. In the practical implementation, the most time-consuming factor resulted to be the placement of the GPCs. GPCs had to be distributed in well visible places for the UAV images around the forest patches and measured with a differential GPS. Nevertheless, the total time spend on the UAV acquisition process was still much less than the TLS data acquisition.

The RMSE for the final geo-referenced UAV data was less than the values obtained by other researchers (J. Zhang et al. 2016). In the future, the time spend on GPCs could also be saved when using high accuracy GPS on board of the UAV. It would also be a solution for areas with limited ground access for GCP placement.

For time-sensitive data acquisition, this can be a big advantage. If the access to an area is limited due to climate or other factors the UAV can cover areas rapidly. This also is an advantage if short interval time series of an area is necessary.

Although the same flight parameters were set for each flight area the processing facility and results did vary between the areas.

In the SfM process the calibration of the images and consequent point cloud construction worked best over plane areas and worst in areas of high complexity such as forest canopy. The recognition of tie points in different images, which is necessary for the calibration process, worked best on planes where the form and colouring of potential tie point features were much less prone to change depending on the viewing angle. Potential tie point features within the tree canopies on the other hand were changing a lot in appearance from one view point to the other. A complex surface as the tree canopy would look very different from different angles and would therefore often not be automatically identified as the same tie point during the SfM processing. An additional problem is that in a forest canopy many features are very similar in shape and colour which makes the unique description of tie points challenging. A unique descriptor nevertheless, is necessary to match the tie points in different images (Bolles & Baker 1987). A very high overlap and therefore only very small changes in viewing angles in neighbouring images is used to avoid this problem (Dandois & Ellis 2013). Even though a very high overlap had been chosen in the flight planning in several flight areas there were problems in the calibration of images due to a lack of automatically identified tie points. In some cases, the inability of automatic calibration was due to complex canopy surfaces while in some cases there were irregularities in the flight path and image spacing which led to a diminished overlap between neighbouring images (Figure 22).

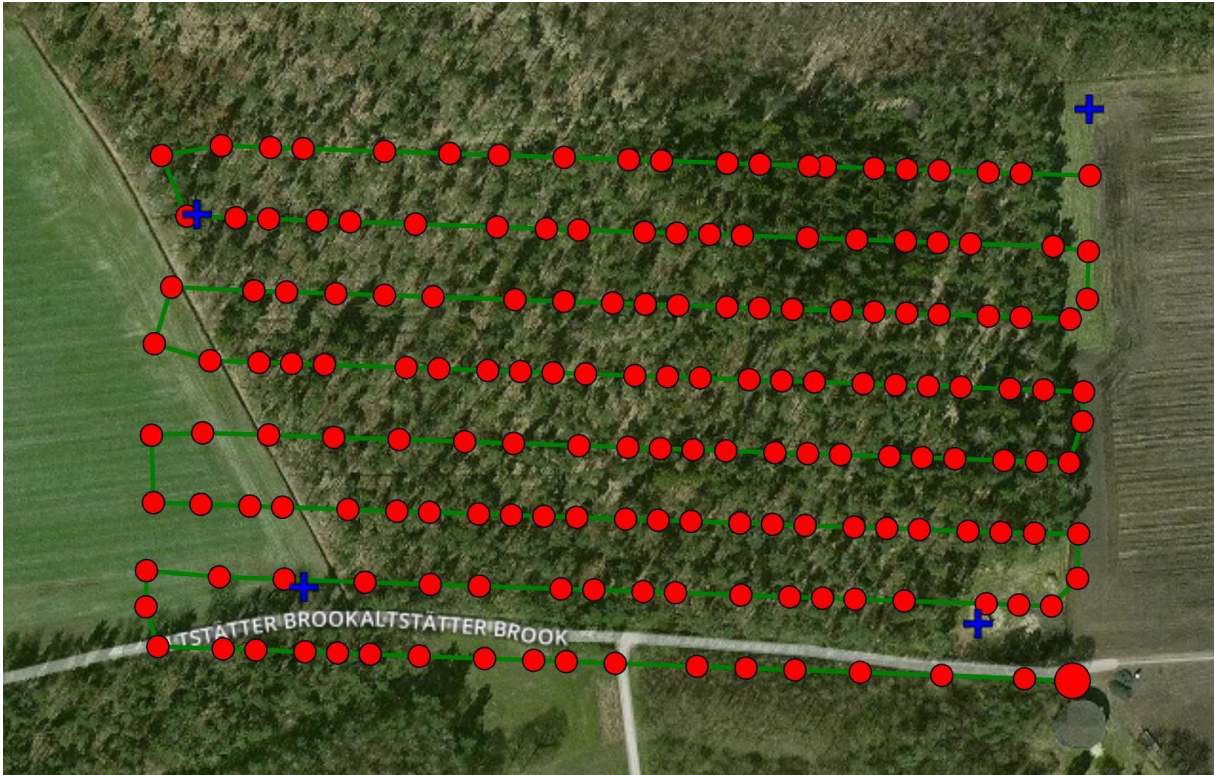


Figure 22: UAV flight area 2 with irregularly spaced image acquisition points (red circles), GCPs (blue crosses) (background image source: Google Maps)

The irregularity of the image spacing is probably due to either inaccuracies of the on-board GPS of the UAV or possibly wind or gusts that either sped up or braked the UAV disrupting the intended flight plan. To avoid these kind of irregularities and ensure a sufficiently high overlap of the images to automatically identify tie-points during a SfM process it would be advisable to fly an area twice with perpendicular flight directions or (also additionally) increase the flying height (Dandois et al. 2015).

Once calibrated the dense point cloud construction could be done without major problems resulting in visually sound 3D representations of the research areas. Although visually sound at first glance, a closer look on the outer edges as well as on the edges to uncalibrated images the point cloud was often much less dense and missing some features completely. This edge effect was a result of insufficient overlap and distortion. The effects can also be seen in the orthomosaic and DSM output which is derived from the point cloud. The orthomosaic and DSM close to these edge areas tended to misrepresent objects or omit them completely (Figure 23 and Figure 24). Some sampling plots were close to these edge areas which might have negatively influenced the accuracy of the OBIA process and analysis.

To ensure a correct representation of objects in the point cloud and the derived orthomosaic and DSM it is therefore important during the flight planning stage to consider generous buffer areas around the research area to avoid the problematic distortion and misrepresentation at the edges of the flight and image covered area.

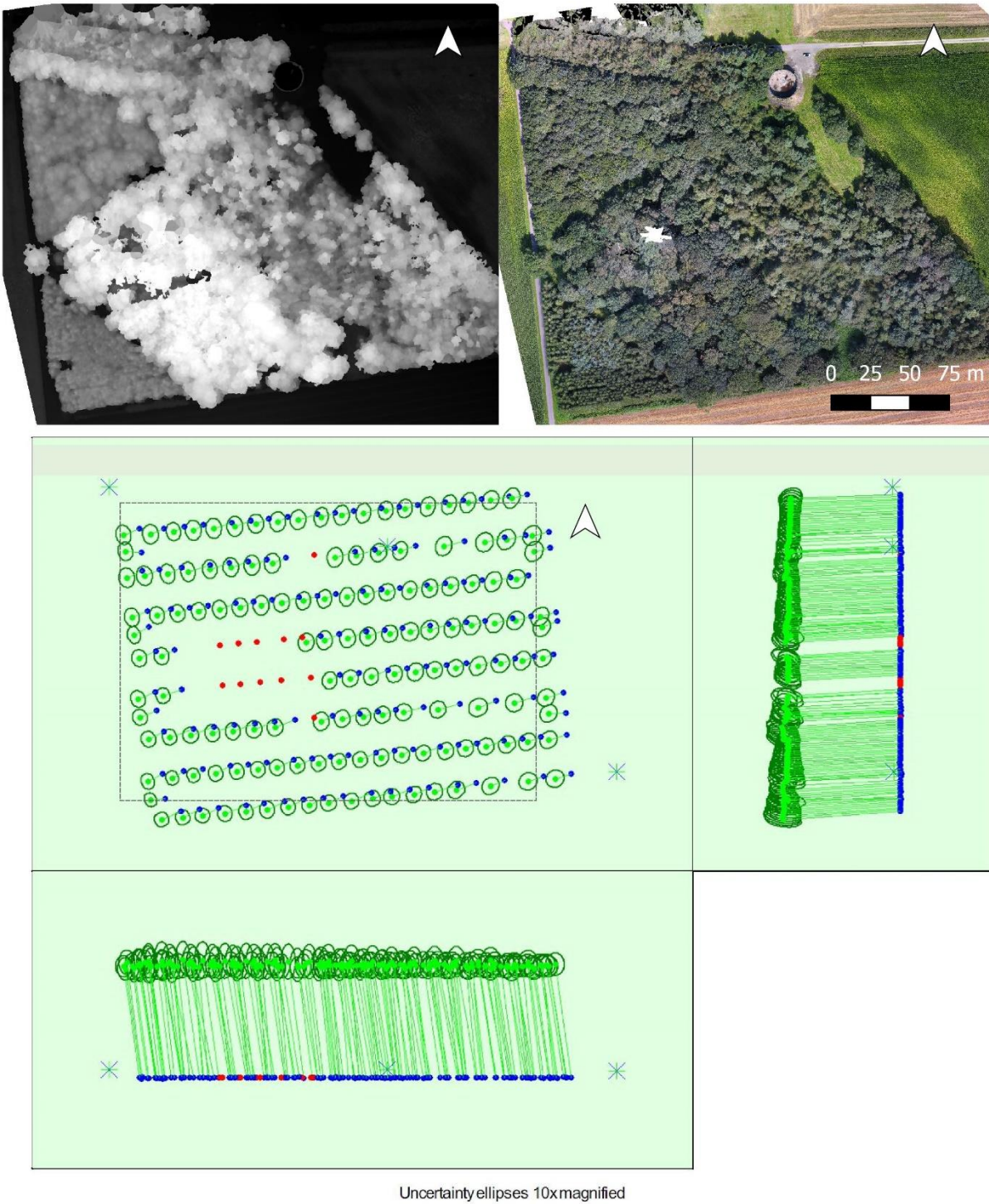


Figure 23: Image calibration results of flight area 1 and the DSM (upper left) and orthomosaic (upper right) derived from the dense point cloud generated in the SfM process (Data: University of Twente, 2017). Lower image: The image calibration results of the SfM process as obtained from the quality report by Pix4D: The grey rectangle marks the scope of the two upper maps. Offset between initial (blue dots) and computed (green dots) image positions as well as the offset between the GCPs initial positions (blue crosses) and their computed positions (green crosses) in the top-view (XY plane), front-view (XZ plane), and side-view (YZ plane). Red dots indicate disabled or uncalibrated images. Dark green ellipses indicate the absolute position uncertainty of the bundle block adjustment result.

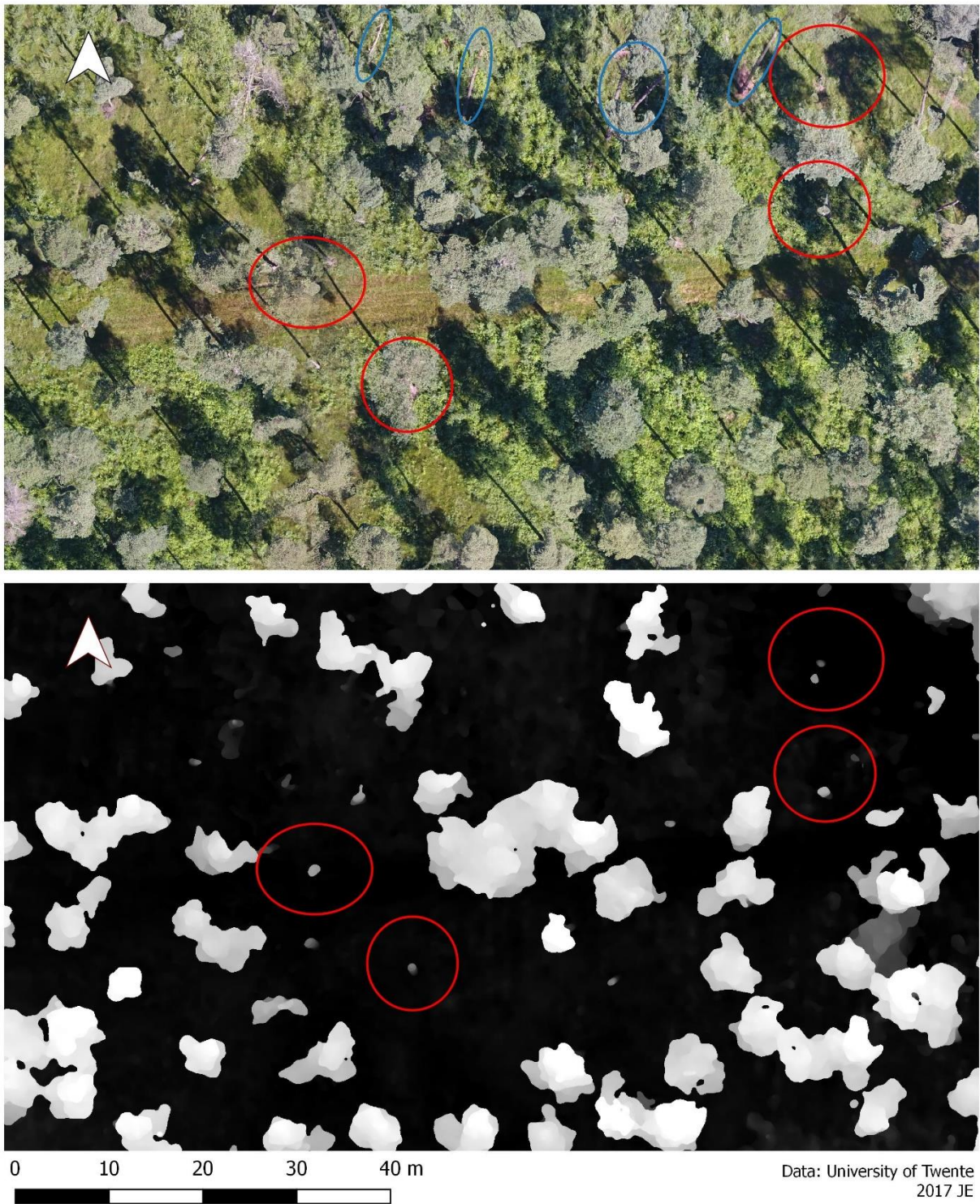


Figure 24: Border area of the flight area 2 DSM (upper map) and orthomosaic (lower map). Showing trees that have not been properly reconstructed during in the SfM process and are therefore incorrectly or partly visible in the orthomosaic and DMS (red circles). The tree locations can be deduced from origin of the shadows of the tree stems in the orthomosaic. Stems of trees (blue circles) that normally should not be visible in the orthomosaic which should give a nadir view only of the tree crowns.

The tree detection and consequently its parameters extraction from the UAV data set are highly dependent on the tree crown delineation. The creation of OBIA rule sets for the crown delineation varied strongly between different plots since they also varied strongly in terms of structure. In this study the individualized approach resulted in visually assessed better fit crown delineations than a uniform approach. This approach has also been used and achieved reasonable results in other studies (Tiede et al. 2006; Burnett et al. 2003). As a general impression, the delineation of low density stands resulted in the most realistic and accurate results while more dense stands had more visually detected inaccuracies.

This was particularly true for the dense stands of mixed or deciduous composition. The delineation of tree crowns in those stands proved most challenging because manual delineation of tree crowns was often ambiguous. Several studies using ALS derived DSMs, spectral information or a combination of both have found that the individual tree delineation in dense deciduous forests leads to non-recognition of up to 76% of the trees, especially of medium to lower canopy trees (Tiede et al. 2006; Jian Yang et al. 2014; Richardson & Moskal 2011). The most challenging stands for the delineation were the dense stands with many different trees (in species, height and crown sizes) and dense deciduous stands with an almost plantation-like structure which resulted in a very uniform and highly intermingled canopy. These stands were prone to over- and under segmentation of the tree crowns. Small trees were often under-segmented while particularly large trees were over-segmented.

Deciduous tree stands tend to have a relatively continuous canopy with intermingling branches in the crowns (Figure 26). The structure of the entangled branches in the deciduous tree stands were visible in the TLS scans where they made the separation of individual trees rather complicated (Figure 26). The coniferous stands in the research area did have more distinguishable canopies that facilitated the extraction of single trees. Although the crowns of scots pine trees were also of relatively irregular shape their delineation also was relatively unambiguous. To a large degree the easy delineation was mostly also due to the very sparse stands (Figure 25) where most scots pine trees were detected and that trees in dense stands were usually much taller than the surrounding tree canopies.



Figure 25: Crown delineation (red) in a low density coniferous plot

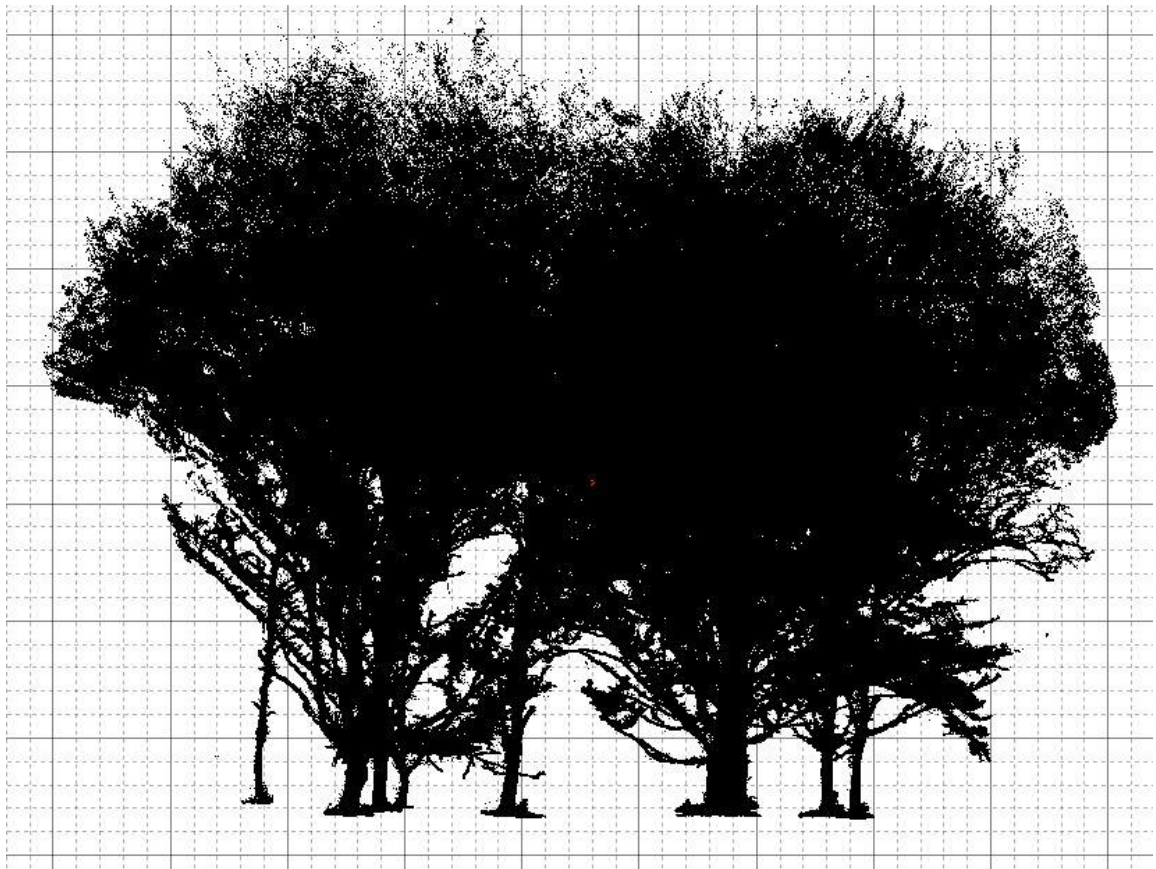
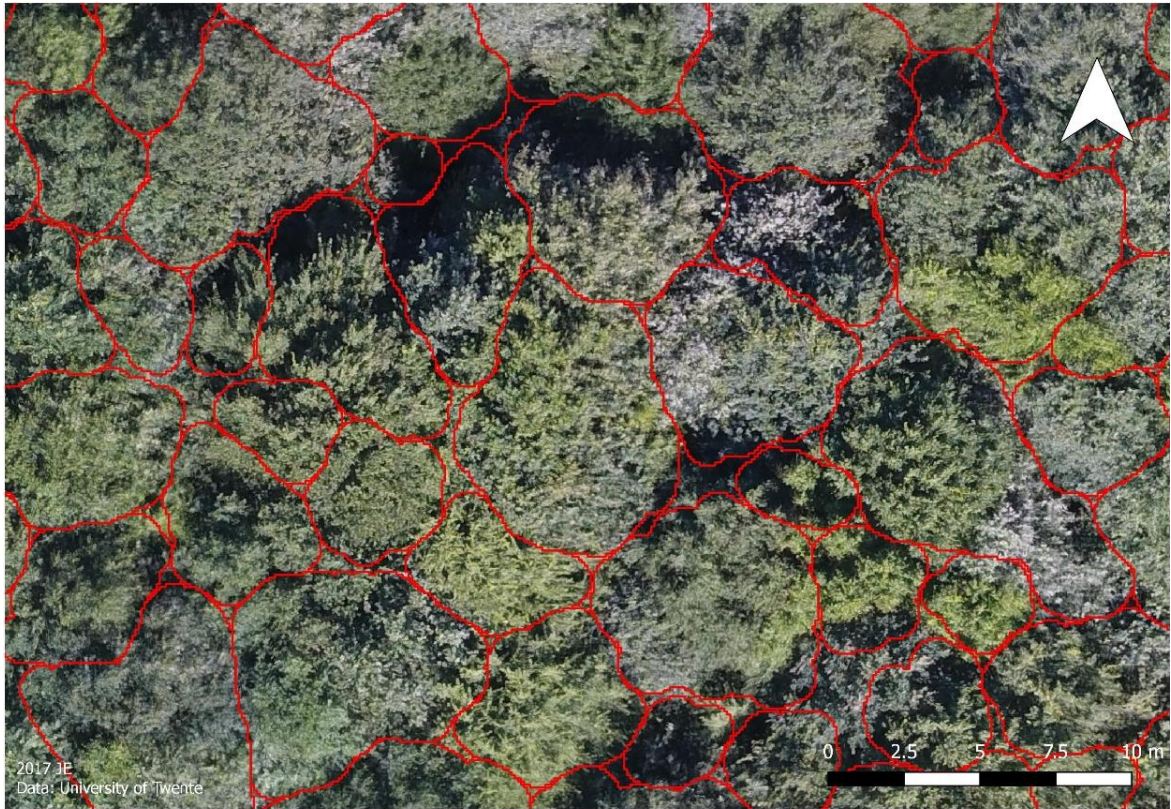


Figure 26: Strongly intermingled crowns of a deciduous plot. Top: UAV derived orthomosaic with crown delineation (red), Bottom: TLS side view of trees of the same plot

4.2. Tree detection and matching

The tree detection ratio from the TLS data was high as it was expected from the experience from other studies (Tansey et al. 2009; Bauwens et al. 2016). Nevertheless, several trees could not be identified from the point clouds probably due to occlusion by other trees or undergrowth.

The percentage of identified tree crowns from the UAV data set shows an overall underestimation of the number of trees in the research area. It could be indicated as a problem of under-segmentation in the OBIA process of outlining the tree crowns or could be caused by undetectable under-canopy trees (Figure 27).

One source of error in the process of position matching of UAV trees and TLS trees came from the inaccuracy of the GPS coordinates for the TLS central scanning position of the sampling plots. While the relative positioning and orientation (North-South-East-West) of the trees in respect to the central scanning point were of high accuracy (i.e., around 2 cm) the GPS location had an expected uncertainty of 3-7 m.

The orthomosaic and DSM generated from the UAV data on the other hand had a higher accuracy due to the geo-referencing with high accuracy GCPs.

To correct the positioning of the TLS centre spots the UAV orthomosaics and DSMs were therefore used as a reference. While maintaining the relative TLS tree positions, the centre was moved manually to adjust to the visually identified centre position in the reference data. In one case, the actual centre location identified in the reference data set was 10 m removed from the GPS measured point.

Although a good visual fit could be reached in most cases, the process was strongly influenced by subjective decisions particularly in dense stands. This could have introduced some inaccuracies in the positioning and thus adding to the uncertainties in the tree matching.



Figure 27: Small under-canopy trees (red) are occluded from above by the crowns of higher surrounding trees (black) and make a recognition in the UAV images impossible.

By choosing the nearest neighbour approach to match tree positions of UAV, TLS and field data and by assuming, that the stem positions coincide with the centre of the crowns there is a distinct possibility of mismatching the trees. By default, and normally a tree develops in a straight and symmetric way. However, due to disturbances (e.g., natural or others) the crown centre points do not always coincides with stem position (Sprauer 2013). Such an irregular tree shape could have led for to a situation where the crown centre point derived from the UAV data was either out of the matching range of 5 m from its real stem position or that the crown or stem were wrongly assigned to another tree stem or crown.

A visual inspection to identify such cases was possible in the low density stands where the individual trees and their position could be distinguished quite well from the UAV derived orthomosaics and DSM. However, in all other plots of the research area this identification was not possible and the matching error caused by irregular tree shapes could not be quantified.

As indicated from the number of identified trees from the UAV data and as was also observed during the TLS data processing there are several small trees in the research area that are smaller than the surrounding trees. Their crowns remain below the canopy and are invisible to the UAV (Figure 27). Although not visible in the UAV data these small trees might have been erroneously matched to UAV delineated trees. Due to positioning errors through the geo-referencing and central crown point assumptions the small trees might in some cases have been the nearest neighbour for a UAV tree position.

To optimize the matching process further investigations and observations are needed to determine how large is the influence of geo-referencing, irregular tree shapes and other factors are on the matching process using the nearest neighbour approach. Other matching approaches could also be considered by introducing an additional criterion to distance. This criterion could for example be based on a relationship of tree height and crown width to the DBH of a tree and matching therefore the most likely pair within a set matching range. This method would require a close study of the allometric relationship of the trees in the study area.

4.3. Tree height extraction and comparison

A major concern in the analysis of the height parameter are the values of the ALS reference values. Although ALS generally known to deliver high accuracy values for tree heights (Tiede et al. 2006), there are studies of ALS measurements with similar resolution as used in this study that show that the ALS height values are around 6.5% smaller than field values (in leave-on conditions) (Verma et al. 2016).

The data was obtained a year previous to the fieldwork with UAV and TLS in February, which is in the leave off season (GeoBasis NRW 2017). Some differences in heights to the UAV and TLS data could have been introduced by the growth of trees between the acquisition of the data sets. The missing foliage is most likely increased the probability of the ALS missing the tree top and reflect off lower branches thus underestimating the tree height as well. The error caused by these problems were not quantified or included in the analysis but their potential impact should be carefully considered.

4.3.1. UAV to field

The RMSE between UAV and ALS height values is very high and the correlation index is rather low (Figure 17). The t-test even revealed that the mean height values are significantly different. As has been discussed previously the ALS as reference data set could have strongly influenced these results.

Furthermore, the UAV height values are depending on the crown delineation (the highest crown value is set as the tree top value) and is therefore affected by inaccuracies occurring in the OBIA process itself and inaccuracies in the data used for it. Inaccurate crown delineations could have led to the potential exclusion of the highest values or also include non-belonging height values larger than the actual height for the respective tree.

The height values were also directly dependent on the DSM created by the SfM process. This also means that the height values were affected by the edge effects which led to a distorted or incomplete point cloud construction and ultimately the inaccurate DSM (Figure 23 and Figure 24).

Particularly two coniferous sampling plots this effect was very noticeable since they were located near the border of the flight areas. Within these sampling plots several trees were only partly or not at all recognizable in the DSM (Figure 24, red circles). The height values for these trees (if they could be delineated at all) were likely to be lower than the actual tree height.

4.3.2. TLS to field

The TLS height values were also found to be significantly different from the reference ALS data displaying a rather large RMSE as well. Reasons for these large differences in height values between TLS and ALS, apart from the problem with the reference data set, could be a result from the problems with the tree matching. In some cases of possible mismatches a sub-canopy tree (e.g. Figure 27) might have been matched with a crown identified from the UAV data. ALS height values as UAV height values are both derived from the forest canopy surface. Sub-canopy trees are occluded from their view. The TLS height value would be much lower than the ALS value which would belong to another tree (visible from above) entirely.

Other inaccuracies in the TLS height values could be derive simply from the occlusion of the actual tree top or also the potentially incorrect subjective decisions taken in the tree extraction process.

4.3.3. UAV to TLS

The direct comparison of UAV and TLS height values does not result in high correlation values. Although Figure 18 shows positively correlated results, the value remains very low at 0.26 and the deviation around this trend was quite substantial. Nevertheless, the results of the paired t-test indicate that the height values of UAV and TLS are not significantly different. The RMSE between UAV and TLS was a meter lower than the RMSE between both data sets and the reference height values which shows a better agreement between UAV and TLS data. Nevertheless, the RMSE value was still rather high indicating large differences in the height values of both sets.

The sources for the high RMSE, although not significant, are in the potential mismatching of trees which is the same problem as with the TLS and ALS height values. The above discussed factors resulting with inaccurate height values from the TLS and UAV data also apply in this case adding to the noise.

4.4. DBH extraction and comparison

4.4.1. UAV to field

While there was no significant difference between the UAV data compared to the field data the collinearity values between the DBH values and the field measurements were rather low (Figure 19). The low collinearity of the UAV DBH values to the field measurements indicate a problem with the estimation of DBH values from the CPA showing overestimations for smaller DBH trees and underestimations for larger DBH ranges.

One source of the under- and over estimations could be in the assumption of a linear relationship between CPA, height and DBH while it could be a non-linear relation. Although the CPA (or sometimes the crown diameter or radius is used) usually has an approximately linear relation to the DBH the relation of DBH and height tends to turn constant for larger DBH values for the most common tree species in the research area (Widlowski et al. 2003). The model is also assuming the same allometric relationship for all tree species in the research area while the species-specific allometric equations are not considered. This can lead to overestimations of DBH values for trees of species with a weaker relationship and to underestimations for species with a stronger relationship.

The sample of matched trees which was used for the model fitting for the estimation of DBH using CPA and height values could also have introduced a bias. Although trees from all sampling plots were used, the sampling in the plot itself was done with a purposeful approach of selecting well fitted crown delineations. The resulting sample could have not been a realistic sample of all matched trees. An over-representation of certain tree species that showed favourable features for delineation in the OBIA process might have occurred. This might have influenced the model fitting. The model might also be influenced by possibly mismatched trees which combine CPA and height values with the DBH value of another tree.

Apart from the inaccuracies originating by the model itself, other factors might also have influenced in the DBH estimations.

The underestimations could be, in part due to the same problem to the possible mismatching of trees. Similar as with the height values, larger crowns could have been matched to smaller sub-canopy trees which are not only smaller in height but most likely in DBH as well. Although in fact a small sub-canopy tree, the delineated UAV crown belongs to a larger tree and the estimations result in a larger DBH value (because of a larger CPA and height).

Under-segmentation of small trees led to over-estimation of DBH values of small trees while over-segmentation of large tree crowns resulted in an underestimation of DBH values for larger trees.

4.4.2. TLS to field

Although there was no significant difference between the TLS DBH values and the field measurements, the collinearity value was at first much lower than expected. The RMSE was very high at over 30 cm. Extreme outliers influenced these values strongly. By removing the five most prominent outliers the collinearity index was much higher (Figure 19). The RMSE was lowered by the outlier removal to 0.079 m which is still

quite large compared to values obtained in other studies, for example DBH estimations with RMSE of 0.019m (Tansey et al. 2009) and 0.024 m (Calders et al. 2015). The differences in accuracy might be in part

due to the differences in the researched stands. In Tansey et al., (2009) the research area was mostly undergrowth free and the trees had almost no low branches that could interfere with the DBH measurements. Calders et al., (2015) studied relatively open eucalyptus stands. Both circumstances could have favoured the measurements since particularly small trees with many branches and trees surrounded by much undergrowth proved to be prone to the extraction of unrealistic DBH values from the TLS data (Tansey et al. 2009). The filter that was applied to remove the noise around the stems did only succeed partly in cleaning out non-stem points. It led to an underestimation of the DBH in some cases because it was also removing points that belonged to the stem.

4.4.3. UAV to TLS

UAV and TLS (without outliers) DBH data were also not significantly different though the RMSE between both was slightly higher than compared to the values with respect to the field measurements. This increased RMSE was probably due to the combination of inaccuracies from the UAV and the TLS DBH extraction.

4.5. Influence of stand composition and density

A general problem of the regression analysis of the influence by stand composition and density is that more than half of the matched trees are from high density deciduous stands (Table 12). For combined stand density and composition classification there were very few or no trees for a sound analysis. The low number or non-existence of trees in classes like the high density coniferous class did skew the analysis further. The skewed sample size of the classes did also result in critical values of collinearity between some classes (Annex 6). A tentative analysis did return low R^2 values and mostly p-values clearly higher than α (Annex 6).

A problem with the regression analysis on tree detection is the relatively small sample size of only 14. The small sample size is because the percentage of matched (UAV) and found (TLS) trees was calculated plot-wise instead of tree wise.

The R^2 for the UAV height regression analysis were the highest for both the analysis of the stand composition ($R^2 = 0.464$) and density ($R^2 = 0.409$). Both composition classes, mixed and deciduous, had a significant impact lowering the percentage of recognized and matched trees each by 28% compared to coniferous stands. These results are similar to those of other studies findings that the delineation of deciduous trees is less accurate than that of coniferous trees (Tiede et al. 2006; Jian Yang et al. 2014; Richardson & Moskal 2011).

The results in this study's analysis were probably also strongly influenced by the fact, that all coniferous stands were of low density since in other studies it has been found that there were also problems with accurate crown delineation of coniferous stands of high density (Korpela et al. 2006).

In the density analysis, the medium and high density did also both have a significant impact compared to the low-density stand lowering the detection and matching by approximately 26 % (high density) and 17 % (medium density).

The TLS tree detection rate was apparently much less impacted by the stand composition and density. Only the density seemed to have some effect but only the medium density factor was found to have a significant impact (around 7% less than in low density stands) on the tree detection. Nevertheless, the general recognition of trees was very high in the TLS data set.

To be able to determine whether the stand composition or its density had more impact on the tree detection, especially from the UAV data, a larger sample size would be required. These sample plots should also include data about the composition density combinations that were not present in this study such as high density coniferous stands.

The rather low R^2 values for both tree height extraction and DBH extraction accuracy seem to indicate, that there might be other factors that influence the accuracy of these parameters. The TLS parameter extraction seemed in general less impacted by the stand composition and density.

One such factor that should be investigated further could be related to the age of trees and how mixed these age groups are within a stand.

5. CONCLUSIONS

In general, the results from this study suggest that the parameters extracted from UAV data are of lower accuracy than the parameters obtained by TLS measurements.

1. *Does processing of the UAV and TLS data lead to the expected raw data for the analysis?*

As expected the tree detection rate from the TLS data was very high (95 %). The number of trees delineated from the UAV data was slightly lower (87.4 %) and decreased further to just over half (56.3 %) of the number of trees counted in the field. The recognition rate of individual trees from the UAV data was lower than in comparable studies.

The UAV data from one flight area could not be calibrated and therefore further processing and analysis could not be done for that area. Problems in the UAV flight planning and data acquisition lead to incomplete or inaccurate results in the UAV data processing.

2. *Is there a significant difference between the UAV derived height values, TLS derived height values and the ALS reference height values?*

There was a significant difference between height values from the reference ALS data and the height values extracted from UAV and TLS data sets. Height values from both data sets, UAV and TLS, were higher than the reference height values from the ALS data set (RMSE UAV 7.7 m, RMSE TLS 6.6 m). UAV and TLS height values were not significantly different from each other.

3. *Is there a significant difference between the UAV derived DBH values, TLS derived DBH values and the DBH values from the field measurements?*

TLS and UAV DBH values were not significantly different from the field measurements.

The accuracy of UAV DBH estimations was higher (RMSE 0.124 m) than the accuracy obtained by the TLS (RMSE 0.334 m) but lower than the TLS DBH accuracy when excluding extreme outliers (0.079 m).

4. *Do forest type and structure influence the tree and parameter (height and DBH) extraction from UAV and TLS data?*

The UAV accuracy of both tree detection and DBH extraction accuracy were both significantly (negatively) influenced by higher density in stands and in stands with higher deciduous tree content. TLS tree detection and DBH value extraction was not influenced by stand composition but partly by stand density. Height values from both data sets were significantly influenced by stand density and composition

LIST OF REFERENCES

- 3D Laser Mapping Ltd., 2012. Riegl VZ-400 Field Guide.
- Aasen, H. et al., 2015. Generating 3D hyperspectral information with lightweight UAV snapshot cameras for vegetation monitoring: From camera calibration to quality assurance. *ISPRS Journal of Photogrammetry and Remote Sensing*, 108, pp.245–259. Available at: <http://linkinghub.elsevier.com/retrieve/pii/S0924271615001938> [Accessed June 23, 2016].
- Alcantarilla, P.F., Bartoli, A. & Davison, A.J., 2012. KAZE Features. *Eur. Conf. on Computer Vision (ECCV)*, pp.214–227.
- Barnston, A.G. & Barnston, A.G., 1992. Correspondence among the Correlation, RMSE, and Heidke Forecast Verification Measures; Refinement of the Heidke Score. *Weather and Forecasting*, 7(4), pp.699–709. Available at: <http://journals.ametsoc.org/doi/abs/10.1175/1520-0434%281992%29007%3C0699%3ACATCRA%3E2.0.CO%3B2> [Accessed May 18, 2017].
- Bauwens, S. et al., 2016. Forest Inventory with Terrestrial LiDAR: A Comparison of Static and Hand-Held Mobile Laser Scanning. *Forests*, 7(6), p.127. Available at: <http://www.mdpi.com/1999-4907/7/6/127> [Accessed August 22, 2016].
- Bezirksregierung Köln, 2016. Digitale Geländemodelle (DGM). Available at: http://www.bezreg-koeln.nrw.de/brk_internet/geobasis/hoeihenmodelle/gelaendemodelle/index.html.
- Bolles, R. & Baker, H., 1987. Chapter 13: Structure From Motion. In *Epipolar-plane Image Analysis: An approach to determining structure from motion*. Available at: <http://academic.research.microsoft.com/Search?query=structure+from+motion>.
- Bolles, R.C., Baker, H.H. & Marimont, D.H., 1987. Epipolar-plane image analysis: An approach to determining structure from motion. *International Journal of Computer Vision*, 1(1), pp.7–55.
- Brown, R., 2007. fitcircle.m - File Exchange - MATLAB Central. *MathWorks- File Exchange*. Available at: <https://nl.mathworks.com/matlabcentral/fileexchange/15060-fitcircle-m> [Accessed May 21, 2017].
- Brown, S., 2002. Measuring carbon in forests: current status and future challenges. *Environmental Pollution*, 116(3), pp.363–372. Available at: <http://ezproxy.utwente.nl:2084/science/article/pii/S0269749101002123> [Accessed May 29, 2017].
- Bucher, I., 2004. Circle fit - File Exchange - MATLAB Central. *MathWorks File Exchange*. Available at: <https://nl.mathworks.com/matlabcentral/fileexchange/5557-circle-fit?focused=5059278&tab=function> [Accessed May 21, 2017].
- Burnett, C., Heurich, M. & Tiede, D., 2003. Exploring Segmentation-based Mapping of Tree Crowns : Experiences with the Bavarian Forest NP Lidar / Digital Image Dataset. In *ScandLaser 2003*. pp. 2003–2003.
- Calders, K. et al., 2015. Nondestructive estimates of above-ground biomass using terrestrial laser scanning S. McMahon, ed. *Methods in Ecology and Evolution*, 6(2), pp.198–208. Available at: <http://doi.wiley.com/10.1111/2041-210X.12301> [Accessed February 17, 2017].
- Dandois, J.P. & Ellis, E.C., 2013. High spatial resolution three-dimensional mapping of vegetation spectral dynamics using computer vision. *Remote Sensing of Environment*, 136, pp.259–276. Available at: <http://linkinghub.elsevier.com/retrieve/pii/S0034425713001326> [Accessed June 23, 2016].
- Dandois, J.P. & Ellis, E.C., 2010. Remote sensing of vegetation structure using computer vision. *Remote Sensing*, 2(4), pp.1157–1176.

- Dandois, J.P., Olano, M. & Ellis, E.C., 2015. Optimal altitude, overlap, and weather conditions for computer vision uav estimates of forest structure. *Remote Sensing*, 7(10), pp.13895–13920.
- DJI, 2016. Phantom 4 - Quick Start Guide. Available at: <http://heliboss.co/DJI-Drones/phantoms/Drone-phantom4/phantom4>.
- Gago, J. et al., 2015. UAVs challenge to assess water stress for sustainable agriculture. *Agricultural Water Management*, 153, pp.9–19. Available at: <http://dx.doi.org/10.1016/j.agwat.2015.01.020>.
- GeoBasis NRW, 2017. TIM-online. *Bezirksregierung Köln*. Available at: http://www.bezreg-koeln.nrw.de/brk_internet/tim-online/index.html [Accessed May 22, 2017].
- Hackenberg, J. et al., 2015. SimpleTree —An Efficient Open Source Tool to Build Tree Models from TLS Clouds. *Forests*, 6(12), pp.4245–4294. Available at: <http://www.mdpi.com/1999-4907/6/11/4245> [Accessed February 3, 2017].
- Husson, E., Lindgren, F. & Ecke, F., 2014. Assessing Biomass and Metal Contents in Riparian Vegetation Along a Pollution Gradient Using an Unmanned Aircraft System. *Water, Air, & Soil Pollution*, 225(6), p.1957. Available at: <http://link.springer.com/10.1007/s11270-014-1957-2> [Accessed June 23, 2016].
- Jakubowski, M. et al., 2013. Delineating Individual Trees from Lidar Data: A Comparison of Vector- and Raster-based Segmentation Approaches. *Remote Sensing*, 5(9), pp.4163–4186. Available at: <http://www.mdpi.com/2072-4292/5/9/4163/> [Accessed April 19, 2017].
- Jian Yang, Yuhong He & Caspersen, J., 2014. A multi-band watershed segmentation method for individual tree crown delineation from high resolution multispectral aerial image. In *2014 IEEE Geoscience and Remote Sensing Symposium*. IEEE, pp. 1588–1591. Available at: <http://ieeexplore.ieee.org/document/6945949/> [Accessed April 19, 2017].
- Kankare, V. et al., 2016. The effect of TLS point cloud sampling on tree detection and diameter measurement accuracy. *Remote Sensing Letters*, 7(5), pp.495–502. Available at: <http://www.tandfonline.com/doi/full/10.1080/2150704X.2016.1157639> [Accessed August 22, 2016].
- Korpela, I., Anttila, P. & Pitkanen, J., 2006. The performance of a local maxima method for detecting individual tree tops in aerial photographs. *International Journal of Remote Sensing*, 27(6), pp.1159–1175. Available at: <http://www.informaworld.com/openurl?genre=article&doi=10.1080/01431160500354070&magic=crossref%7C%7CD404A21C5BB053405B1A640AFFD44AE3> [Accessed April 22, 2017].
- Laar, A. van & Akça, A., 2007. *Forest Mensuration*, Dordrecht: Springer Netherlands. Available at: <http://link.springer.com/10.1007/978-1-4020-5991-9> [Accessed August 19, 2016].
- van Leeuwen, M. & Nieuwenhuis, M., 2010. Retrieval of forest structural parameters using LiDAR remote sensing. *European Journal of Forest Research*, 129(4), pp.749–770.
- Liang, X. et al., 2016. Terrestrial laser scanning in forest inventories. *ISPRS Journal of Photogrammetry and Remote Sensing*, 115, pp.63–77.
- Lucas, R.M., Mitchell, A.L. & Armston, J., 2015. Measurement of Forest Above-Ground Biomass Using Active and Passive Remote Sensing at Large (Subnational to Global) Scales. *Current Forestry Reports*, 1(3), pp.162–177. Available at: <http://link.springer.com/10.1007/s40725-015-0021-9> [Accessed June 23, 2016].
- MacFaden, S.W. et al., 2012. High-resolution tree canopy mapping for New York City using LIDAR and object-based image analysis. *Journal of Applied Remote Sensing*, 6(1), pp.63567–1. Available at: <http://remotesensing.spiedigitallibrary.org/article.aspx?doi=10.1117/1.JRS.6.063567> [Accessed April 19, 2017].

- Olofsson, K., Holmgren, J. & Olsson, H., 2014. Tree Stem and Height Measurements using Terrestrial Laser Scanning and the RANSAC Algorithm. *Remote Sensing*, 6(5), pp.4323–4344. Available at: <http://www.mdpi.com/2072-4292/6/5/4323/> [Accessed April 21, 2017].
- Ota, T. et al., 2015. Aboveground Biomass Estimation Using Structure from Motion Approach with Aerial Photographs in a Seasonal Tropical Forest. *Forests*, 6(11), pp.3882–3898. Available at: <http://www.mdpi.com/1999-4907/6/11/3882/> [Accessed June 8, 2016].
- Rasel, S.M.M. et al., 2017. Proxies for soil organic carbon derived from remote sensing. *International Journal of Applied Earth Observation and Geoinformation*, 59, pp.157–166. Available at: <http://linkinghub.elsevier.com/retrieve/pii/S0303243417300673> [Accessed May 1, 2017].
- Ravindranath, N.H. & Ostwald, M., 2008. *Carbon Inventory Methods Handbook for Greenhouse Gas Inventory, Carbon Mitigation and Roundwood Production Projects*, Dordrecht: Springer Netherlands. Available at: <http://link.springer.com/10.1007/978-1-4020-6547-7> [Accessed August 19, 2016].
- Richardson, J.J. & Moskal, L.M., 2011. Strengths and limitations of assessing forest density and spatial configuration with aerial LiDAR. *Remote Sensing of Environment*, 115(10), pp.2640–2651.
- RIEGL Laser Measurement Systems GmbH, 2017. RIEGL - Produktdetail - RIEGL VZ-400. Available at: <http://www.riegl.com/products/terrestrial-scanning/produktdetail/product/scanner/5/> [Accessed May 23, 2017].
- Rosenqvist, Å. et al., 2003. A review of remote sensing technology in support of the Kyoto Protocol. *Environmental Science and Policy*, 6(5), pp.441–455. Available at: <http://linkinghub.elsevier.com/retrieve/pii/S1462901103000704> [Accessed June 8, 2016].
- Rutishauser, E. et al., 2013. Generic allometric models including height best estimate forest biomass and carbon stocks in Indonesia. *Forest Ecology and Management*, 307, pp.219–225.
- Schiffman, R., 2014. Drones Flying High as New Tool for Field Biologists. *Science*, 344(6183). Available at: <http://science.sciencemag.org/content/344/6183/459.full> [Accessed April 10, 2017].
- Sprauer, S., 2013. *Modelle zur Abbildung asymmetrischer Kronen-formen und zur Beschreibung der Zuwachsleistung für sechs Baumarten in Nordwestdeutschland*. Georg-August-Universität Göttingen.
- Stefanik, K. V. et al., 2011. UAV-Based Stereo Vision for Rapid Aerial Terrain Mapping. *GIScience & Remote Sensing*, 48(1), pp.24–49.
- Suárez, J.C. et al., 2005. Use of airborne LiDAR and aerial photography in the estimation of individual tree heights in forestry. *Computers & Geosciences*, 31(2), pp.253–262.
- Tang, L. & Shao, G., 2015. Drone remote sensing for forestry research and practices. *Journal of Forestry Research*, 26(4), pp.791–797. Available at: <http://link.springer.com/10.1007/s11676-015-0088-y> [Accessed June 23, 2016].
- Tansey, K. et al., 2009. Estimating tree and stand variables in a Corsican Pine woodland from terrestrial laser scanner data. *International Journal of Remote Sensing*, 30(19), pp.5195–5209. Available at: <http://www.tandfonline.com/doi/abs/10.1080/01431160902882587> [Accessed February 17, 2017].
- Tiede, D., Lang, S. & Hoffmann, C., 2006. SUPERVISED AND FOREST TYPE-SPECIFIC MULTI-SCALE SEGMENTATION FOR A ONE-LEVEL-REPRESENTATION OF SINGLE TREES. In *1st International Conference on Object-based Image Analysis (OBIA 2006)*. Available at: http://www.isprs.org/proceedings/xxxvi/4-c42/Papers/02_Potential and problems of multiscale representation/OBIA2006_Tiede_Lang_Hoffmann.pdf [Accessed April 19, 2017].

- Verma, N.K. et al., 2016. Comparison of canopy volume measurements of scattered eucalypt farm trees derived from high spatial resolution imagery and LiDAR. *Remote Sensing*, 8(5).
- Wallace, L. et al., 2016. Assessment of Forest Structure Using Two UAV Techniques: A Comparison of Airborne Laser Scanning and Structure from Motion (SfM) Point Clouds. *Forests*, 7(3), p.62. Available at: <http://www.mdpi.com/1999-4907/7/3/62> [Accessed August 25, 2016].
- West, P.W., 2009. *Tree and Forest Measurement*, Berlin, Heidelberg: Springer Berlin Heidelberg. Available at: <http://link.springer.com/10.1007/978-3-540-95966-3> [Accessed June 21, 2016].
- Widłowski, J.-L. et al., 2003. *Allometric Relationships of Selected European Tree Species*,
- Wirth, C., Gleixner, G. & Heimann, M. eds., 2009. *Old-Growth Forests*, Berlin, Heidelberg: Springer Berlin Heidelberg. Available at: <http://link.springer.com/10.1007/978-3-540-92706-8> [Accessed June 21, 2016].
- Zhang, J. et al., 2016. Seeing the forest from drones: Testing the potential of lightweight drones as a tool for long-term forest monitoring. *Biological Conservation*, 198, pp.60–69. Available at: <http://linkinghub.elsevier.com/retrieve/pii/S0006320716301100> [Accessed June 8, 2016].
- Zhang, W. et al., 2016. Efficient registration of terrestrial LiDAR scans using a coarse-to-fine strategy for forestry applications. *Agricultural and Forest Meteorology*, 225(September), pp.8–23. Available at: <http://linkinghub.elsevier.com/retrieve/pii/S0168192316302611>.

Annex1

Fieldwork procedure

The procedure followed during the fieldwork was the following:

1. Find location of first plot using the GPS and the coordinate list.
 - a. If it is not the first day in the field: find the position of the last plot of the previous day.
 - b. Continue looking for next plot location in a structured way (north-south, east-west).
2. When scan centre position is found:
 - a. Place reflectors (evenly distributed in horizontal and vertical component).
 - b. Mark and count all trees (DBH > 10 cm) in plot with numbered targets and reflectors.
 - c. Take GPS measurement of scanning position.

TLS data acquisition:

- a. Level TLS.
- b. Create new scanning position (name accordingly).
- c. Enter scan settings (Panorama 40 for resolution).
- d. Start scanning process.

Manual measurements:

- a. Identify tree species (based on personal knowledge, take pictures of unknown tree species for later identification).
 - b. Measure DBH (1.3 m above ground).
3. Using a compass, find the surrounding plot positions.
 - a. Take 4 surrounding plot positions (90 degrees) at approximately 12.6 m distance from the centre position
 4. When found, scan surrounding plot positions.
Repeat 2a – 2f.
 5. When finished, move to next plot. Repeat from step 2.

Annex 2

Table 11: Standard Deviation (StDev) for scan registration in TLS plots. Calculated by using reflectors as tie points for scan registration by using a least square approach in RiSCAN PRO.

Plot	StDev (m)
20160908_1	0.051
20160912_1	0.060
20160912_2	0.019
20160919_2	0.014
20160920_1	0.015
20160920_2	0.016
20160922_1	0.026
20160922_2	0.018
20160923_1	0.025
20160923_2	0.011
20160923_4	0.011
20160924_1	0.014
20160924_2	0.011
20160926_1	0.016
20160926_2	0.012
Average	0.021
Min	0.011
Max	0.060

Annex 3

Flight plans



Figure 28: Flight plan (green line and red image taking positions) and GCPs (blue crosses) for UAV flight area 1



Figure 29: Flight plan (green line and red image taking positions) and GCPs (blue crosses) for flight area 3

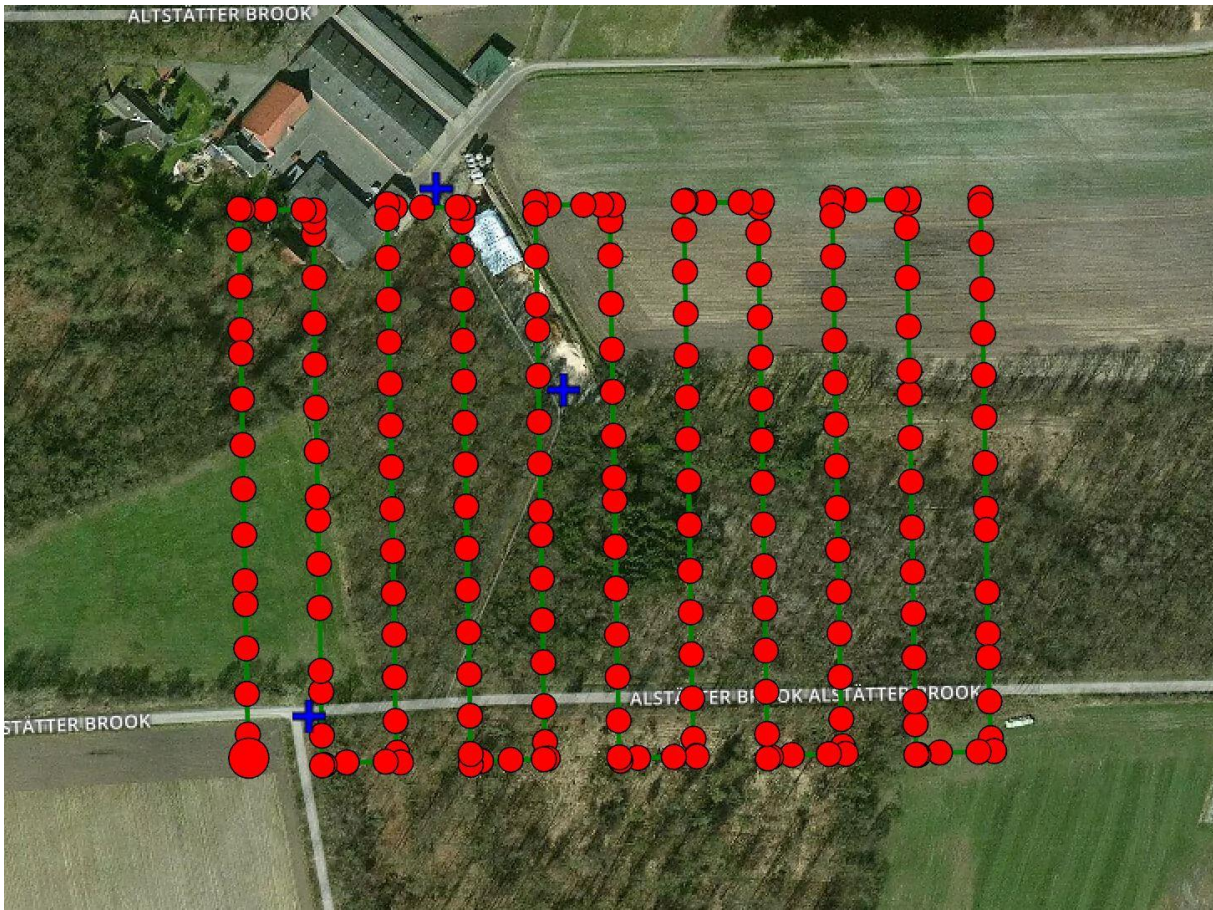


Figure 30: Flight plan (green line and red image taking positions) and GCPs (blue crosses) for flight area 5

Annex 4

Composition and density class per plot

Table 12: Composition class, density class and number of matched trees per plot

Plot	Number of matched trees	Density	Composition
0908_1	9	Medium	Mixed
0912_1	17	Medium	Mixed
0912_2	22	High	Deciduous
0922_1	7	Low	Coniferous
0922_2	5	Low	Coniferous
0923_1	7	Low	Coniferous
0923_2	19	High	Deciduous
0923_3	14	Medium	Deciduous
0924_1	12	Medium	Deciduous
0924_2	22	High	Deciduous
0926_1	12	High	Mixed
0926_2	12	High	Deciduous
1024_1	8	Low	Mixed
1026_1	18	High	Deciduous
Total	184	-	-

Annex 5

DTM and CHM processing

Import ascii point elevation data

Clip point elevation vector

Rasterize point elevation vector (using pointtoraster tool in ArcGIS) using automatic cell-size

Clip elevation raster using plot extends

Resample (bilinear interpolation method) individual dtms using respective dsm plot for resolution

Substract DTM from respective DSM to obtain CHM

Annex 6

Regression analysis for combined composition and density

Table 13: Results of regression analysis combining density and composition classes

p-values ->		Stand composition and density				
		R ² adj.	Mix.	Dec.	Med.	High
Tree det.	UAV	0.474	0.126	0.329	0.814	0.341
	TLS	0.098	1	0.739	0.158	0.336
	pos.	0.069	0.016	0.008	0.565	0.660
Height	UAV-ALS	0.179	0.003	0.012	0.825	0.042
	TLS-ALS	0.117	0.886	0.838	0.016	0.225
	UAV-TLS	0.139	0.035	0.066	0.163	0.234
DBH	UAV-field	0.124	0.049	0.104	0.688	0.177
	TLS-field	0.019	0.330	0.243	0.018	0.036
	UAV-TLS	0.059	0.781	0.560	0.016	0.013